

RGBT-Ground Benchmark: Visual Grounding Beyond RGB in Complex Real-World Scenarios

Tianyi Zhao¹, Jiawen Xi¹, Linhui Xiao², Junnan Li¹, Xue Yang³, Maoxun Yuan¹, Xingxing Wei¹

¹ Beihang University, ²Pengcheng Laboratory, ³Shanghai Jiao Tong University

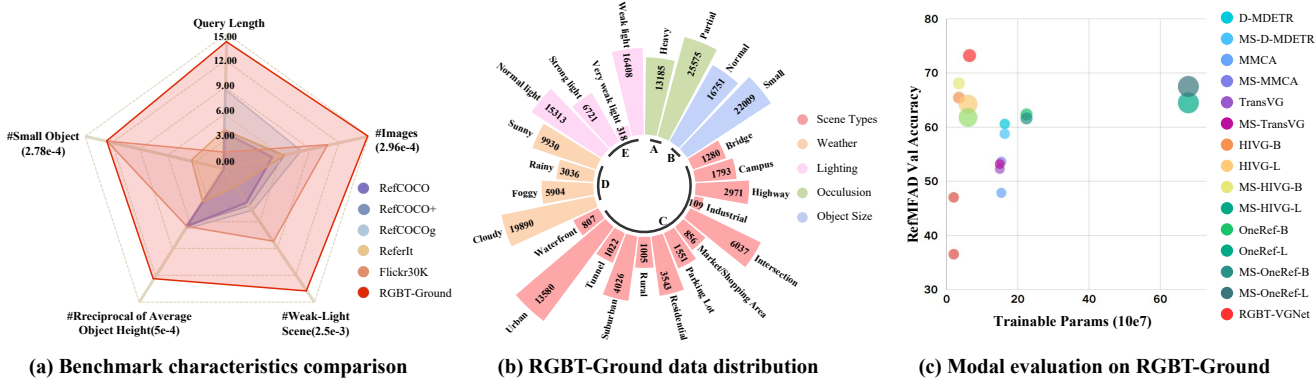


Figure 1. Comparative overview of the RGBT-Ground benchmark and its evaluation of representative grounding method. (a) Comparative characteristics of RGBT-Ground against classical visual grounding benchmarks. (b) Data distribution of lighting, occlusion, object, weather, and scene types. (c) Method evaluation on RGBT-Ground.

Abstract

Visual Grounding (VG) aims to localize specific objects in an image according to natural language expressions, serving as a fundamental task in vision–language understanding. However, existing VG benchmarks are mostly derived from datasets collected under clean environments, such as COCO, where scene diversity is limited. Consequently, they fail to reflect the complexity of real-world conditions, such as changes in illumination, weather, etc., that are critical to evaluating model robustness and generalization in safety-critical applications. To address these limitations, we present RGBT-Ground, the first large-scale visual grounding benchmark built for complex real-world scenarios. It consists of spatially aligned RGB and Thermal infrared (TIR) image pairs with high-quality referring expressions, corresponding object bounding boxes, and fine-grained annotations at the scene, environment, and object levels. This benchmark enables comprehensive evaluation and facilitates the study of robust grounding under diverse and challenging conditions. Furthermore, we establish a unified visual grounding framework that supports both uni-modal (RGB or TIR) and multi-modal (RGB–TIR) visual inputs. Based on it, we propose RGBT-VGNet, a simple yet effective baseline for fusing complementary visual modalities

to achieve robust grounding. We conduct extensive adaptations to the existing methods on RGBT-Ground. Experimental results show that our proposed RGBT-VGNet significantly outperforms these adapted methods, particularly in nighttime and long-distance scenarios. All resources will be publicly released to promote future research on robust visual grounding in complex real-world environments.

1. Introduction

Visual Grounding (VG) aims to localize objects in an image based on natural language descriptions, enabling the integration of vision and language information. By effectively combining the semantic richness of language with visual context, VG holds significant potential for advancing intelligent human-agent interactions across a wide range of applications, such as autonomous driving [46], embodied robotics [11], and UAV remote sensing [45]. In recent years, VG benchmarks (e.g., RefCOCO/+g [26, 43], ReferIt [17], Flickr30K [27], Ref-ZOM [16], MC-Bench [38], Crops-ref [3], D³ [37], gRefCOCO [21], etc.) and powerful vision-language pre-trained models (e.g., CLIP [28], BEIT3 [32], LLaVA [23], etc.) have greatly advanced the field, improving the accuracy of VG methods.

Despite remarkable progress in visual grounding, existing VG benchmarks still suffer from several critical limitations that hinder their applicability in real-world scenarios: **❶ Limited Scene Complexity.** Most benchmarks are built from datasets collected in clean environments, typically featuring centered and salient objects. Such settings fail to reflect the cluttered and dynamic nature of real-world scenes. **❷ Lack of Environmental Diversity.** Current datasets rarely include challenging conditions such as varying illumination, adverse weather, or nighttime scenes, leading to poor generalization in all-day and all-weather applications. **❸ Insufficient Object Diversity.** Small, distant, and occluded objects are underrepresented, making it difficult to evaluate model robustness in safety-critical domains such as autonomous driving and embodied perception.

To bridge the gap between existing benchmarks and real-world challenges, we propose a multi-modal **RGB–Thermal Visual Grounding** benchmark named **RGBT-Ground**. To our knowledge, it is the first large-scale benchmark designed for complex real-world visual grounding with multi-visual modality. As shown in Figure 1 (a) and (b), RGBT-Ground contains approximately 40K spatially aligned RGB and thermal infrared (TIR) images with fine-grained annotations at three levels: scene-level (13 scene types), environment-level (4 illumination conditions and 4 weather conditions), and object-level (object size and occlusion). Compared with previous benchmarks, it includes a substantially higher proportion of small objects (57.7%) and low-light samples (23.1%), along with more diverse referring expressions (14.24 words per query on average), making it a more comprehensive and challenging resource for multi-modal visual input grounding research.

Existing visual grounding methods are primarily designed for uni-modal visual input and cannot be directly applied to multi-modal visual input settings. So we develop a unified visual grounding framework, named **RGBT-VG**, that adapts several representative uni-modal VG methods to support multi-modal visual inputs. Based on the framework, we further propose **RGBT-VGNet**, a baseline built upon a pretrained vision–language model, enabling accurate object localization by leveraging complementary information across RGB and TIR visual modalities. As shown in Figure 1 (c), RGBT-VGNet achieves state-of-the-art performance while maintaining a reasonable number of trainable parameters. Specifically, it incorporates two key components: (1) Asymmetric Modality Adaptation, which mitigates modality-specific visual feature discrepancies, and (2) Language-Aware Visual Synergy, which enhances cross-modal interactions guided by referring expressions. These designs enable robust grounding under diverse and challenging conditions, providing a solid reference for future multi-modal visual input grounding research.

To comprehensively evaluate the robustness of exist-

ing methods and the effectiveness of our proposed benchmark and framework, we conduct large-scale experiments on RGBT-Ground, comprising over **60** experimental configurations. Specifically, our evaluation covers two experimental settings, three modality combinations, and seven baseline methods along with their variants or extensions, tested across three sub-datasets of the RGBT-Ground Benchmark, RefFLIR, RefM³FD, and RefMFAD. The results reveal that current VG models exhibit limited generalization under complex real-world conditions. When restricted to unimodal input, performance significantly degrades in nighttime, low-light, and small-object scenarios, whereas multi-modal visual input models exhibit significant robustness.

To highlight the significance of our research, we summarize the main contributions as follows:

- **Benchmark.** We present **RGBT-Ground**, the first large-scale multi-modal RGBT visual grounding benchmark designed for complex real-world scenarios.
- **Framework and Baseline.** We develop **RGBT-VG**, a unified framework for RGBT visual grounding, which extends existing representative VG models to support multi-modal visual inputs. We further propose a strong baseline method, **RGBT-VGNet**, to facilitate future research.
- **Evaluation.** We establish an evaluation protocol for RGBT visual grounding and conduct large-scale experiments on RGBT-Ground across over 60 configurations.
- **Resources.** We will release all RGBT-Ground benchmark data, framework codes, model implementations, and evaluation toolkits to promote repeatability and drive further development of multi-modal visual input grounding.

2. Related Works

2.1. Visual Grounding in the RGB Domain

With the rise of deep learning [13], the visual grounding field has rapidly advanced [2, 10, 18, 31, 40], driven by increasingly powerful visual and language representation models [7, 9, 30]. Early approaches, such as ReSC [39], adopted CNN-based region-ranking pipelines. Later, transformer-based architectures, including TransVG [6], QRNet [42], and D-MDETR [29] enabled end-to-end grounding with stronger global and contextual reasoning. The development of vision–language pre-training further boosted performance, as demonstrated by methods like CLIP-VG [33] and HiVG [35], which leverage large-scale image–text alignment to enhance cross-modal representations. Existing VG methods are mainly designed and evaluated on RGB-only datasets, causing them to be sensitive to illumination changes and adverse weather, limiting robustness in challenging real-world conditions.

Table 1. Comparison of RGBT-Ground with existing benchmarks. This table highlights key characteristics such as modality and the proportion of weak-light scenes and small objects.

Benchmark	Modality	Typical res.	#Instance	#Weak-light	#Small Object	Query Length	Data Source
Flickr30K [27]	RGB	500x375	276,000	2,588 (0.9%)	0 (0.0%)	1.59	Flickr [17], IAPR-TC [12]
ReferIt [17]	RGB	480x360	96,654	2,588 (2.77%)	0 (0.0%)	3.45	IAPR-TC [12]
RefCOCO [43]	RGB	640x480	50,000	3,068 (6.1%)	0 (0.0%)	3.49	MSCOCO [20]
RefCOCO+ [43]	RGB	640x480	49,856	1,415 (2.8%)	5,998 (12.0%)	3.58	MSCOCO [20]
RefCOCOg [26]	RGB	640x480	49,822	5,342 (10.7%)	22,609 (45.4%)	8.47	MSCOCO [20]
RGBT-Ground (ours)	RGB+TIR	640x512	38,760	8,971 (23.1%)	22,831 (57.7%)	14.24	FLIR [48], M ³ FD [24], MFAD [15]

Table 2. Dataset composition for RGBT-Ground Benchmark, detailing the number of instances from each source and the split across Train, Val, Test, and specialized test subsets.

Benchmark	Sub-dataset	#Ins	Train			Test			TestA	TestB	TestC	Data Source
			Val	Test	Test	Test	Test	Test				
RGBT-Ground	RefFLIR	9,712	7,000	608	2,104	837	640	986	FLIR [48]	M3FD [24]	MFAD [15]	
	RefM ³ FD	7,548	3,604	168	3,776	1,232	1,094	1,848				
	RefMFAD	21,500	16,000	1,256	4,244	789	2,452	2,550				
	Total	38,760	26,604	2,032	10,124	2,858	4,186	5,384				ALL

2.2. Visual Grounding beyond RGB domain

Existing 2D visual grounding methods rely almost exclusively on RGB imagery, making them sensitive to illumination changes and adverse weather conditions. While some works explore extending VG beyond RGB, for example, by incorporating depth information in RGB-D settings [4, 22, 25], their formulations target 3D environments and are not directly applicable to 2D grounding. Moreover, depth sensing often degrades under low-light or adverse weather conditions, limiting its effectiveness as a complementary modality for robust 2D grounding. In contrast, thermal imaging is inherently illumination-invariant and provides stable cues in nighttime, low-light, and adverse weather conditions scenarios, motivating the exploration of RGB–Thermal (RGBT) visual grounding.

Despite RGBT perception has made notable progress in detection [8, 44, 50, 51] and segmentation [19, 47, 49], RGBT visual grounding remains largely unexplored. This gap motivates the construction of our RGBT-Ground benchmark, which is a large-scale 2D visual grounding benchmark that offers aligned RGB–TIR image pairs, high-quality bounding boxes, precise referring expressions, and fine-grained annotations. This benchmark enables systematic evaluation of multi-sensor grounding models under diverse and challenging real-world conditions.

3. RGBT-Ground Benchmark

3.1. Overview

RGBT-Ground is the first large-scale RGB–Thermal visual grounding benchmark specifically designed for complex and real-world scenarios. It comprises over 40K images (21,535 RGBT image pairs) captured in diverse real-world environments, consisting of spatially aligned or weakly aligned RGB and TIR image pairs. Each image pair is annotated with high-quality natural language re-

Table 3. Statistics of lighting and weather conditions in the RGBT-Ground. The distribution demonstrates that LVLM-based annotations are physically consistent with real-world conditions.

Light-Weather	Foggy (FY)	Rainy (RY)	Sunny (SY)	Cloudy (CY)
Very Weak (VWL)	71 (0.33%)	29 (0.13%)	0 (0.00%)	101 (0.47%)
Weak (WL)	2,754 (12.79%)	1,298 (6.03%)	14 (0.07%)	4,704 (21.84%)
Normal (NL)	521 (2.42%)	150 (0.70%)	2,191 (10.19%)	6,157 (28.59%)
Strong (SL)	4 (0.02%)	0 (0.00%)	3,152 (14.64%)	389 (1.81%)

ferring expressions, corresponding object bounding boxes, and fine-grained annotations. As illustrated in Figure 2, RGBT-Ground provides comprehensive annotations covering scene types, illumination conditions, weather variations, object sizes, and occlusion levels—factors that frequently occur in practical applications but remain largely underrepresented in existing benchmarks. These characteristics substantially enhance both the scenario realism and task difficulty of the dataset, thereby encouraging the development of more robust and generalizable visual grounding models.

Overall, RGBT-Ground introduces several key advances over existing visual grounding benchmarks:

- **Fine-grained multi-level annotations.** Covering scene-, environment-, and object-level attributes for comprehensive contextual understanding.
- **Off-central object distribution.** Objects appear in more diverse and realistic spatial positions, better reflecting real-world perception challenges.
- **Increased diversity of challenging samples.** Including a higher proportion of nighttime, low-light, and long-range instances for robust evaluation (as shown in Table 1).
- **Paired multi-modal visual RGBT images.** Enabling reliable grounding across complex real-world scenarios.

3.2. Data Collection, Filtering and Captioning

Collection. We begin by collecting multi-modal object detection datasets [15, 24, 48] covering diverse real-world scenarios. As summarized in Tables 1 and 2, these data sources provide spatially aligned RGB and TIR image pairs, encompassing a wide spectrum of weather, lighting, and scene complexities. Each image pair is accompanied by object-level bounding box annotations, which ensure accurate multi-modal analysis and visual-language grounding.

Filtering. The collected data undergo a rigorous filtering process to ensure high quality and suitability for visual grounding research. We establish a comprehensive filtering pipeline covering three key aspects:

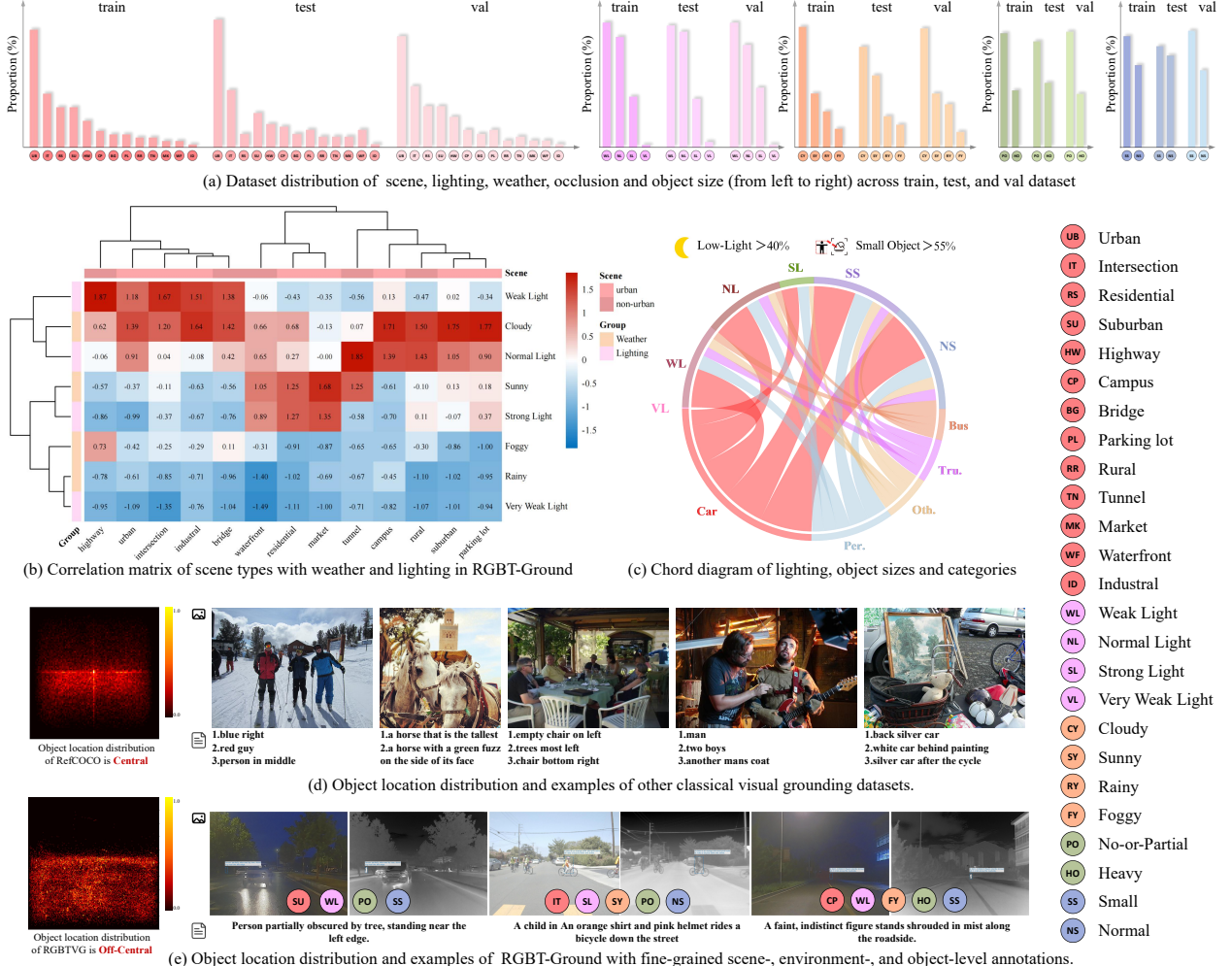


Figure 2. Overview and characteristic analysis of the proposed RGBT-Ground benchmark. (a–c) present dataset distributions and correlations across scene, environment, and object level annotation, while (d–e) show object location distributions and representative samples. Compared with prior visual grounding datasets, RGBT-Ground captures more realistic conditions with off-center, small, and occluded objects under low-light and adverse weather, supported by paired RGB–Thermal imagery.

- Object visibility and scale: We exclude excessively small targets that occupy only a few pixels, as they provide insufficient semantic information for reliable annotation and meaningful textual descriptions.
- Cross-modality alignment accuracy: Image pairs exhibiting significant spatial misalignment between the RGB and TIR modalities are removed to ensure consistent cross-sensor correspondence.
- Category balance: Long-tailed or underrepresented categories (e.g., *dog* in FLIR and *lamp* in M3FD) are filtered out to alleviate class imbalance.

For the retained samples, we further select the largest instance of each object category per image pair to enhance annotation clarity and preserve cross-modality consistency. This filtering process ensures that RGBT-Ground faithfully captures the complexity, diversity, and challenges inherent in real-world deployment scenarios.

Captioning. As shown in Figure 3, we employ the Qwen-VL large vision–language model (LVLM) API to generate high-quality textual annotations in the captioning stage. Carefully designed prompts are used to produce two types of labels: (1) Object referring expressions, (2) Scene-, environment-, and object-level annotations. The specific prompt templates are provided in the *supplementary material*. After automatic captioning, a hierarchical random sampling strategy is applied for human verification and refinement to ensure annotation accuracy and consistency. As shown in Table 3, we further perform statistical validation to confirm the physical reasonability of LVLM-generated labels with lighting and weather distributions matching real-world patterns. This dual-level annotation scheme enriches RGBT-Ground sample with comprehensive semantic and contextual information, thereby supporting robust visual grounding across diverse and challenging environments.

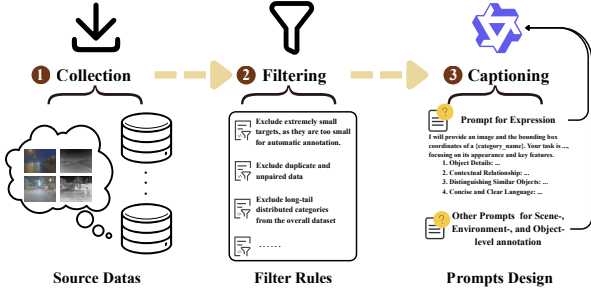


Figure 3. Illustration of the RGBT-Ground data preparation pipeline. The process consists of three main stages: (1) Collection of multi-modal RGBT source data; (2) filtering based on the pre-defined rules, and (3) captioning using carefully designed prompts with the Qwen-VL [1] model.

3.3. Evaluation Protocol

Subset Split. As summarized in Table 2, all instances are divided into train, val, and test subsets following the source data split. The test set is further partitioned into more specialized subsets: **TestA**, covering normal-size (NS) targets under normal-light (NL) and strong-light (SL) conditions; **TestB**, focusing on nighttime scenarios with weak-light (WL) and very-weak-light (VL) environments; and **TestC**, containing small-size (SS) targets. Additional scene-, weather-, and occlusion-based splits, and corresponding evaluation results, will be provided in the supplementary material. This splitting strategy facilitates a fine-grained evaluation of model performance across diverse difficulty levels and environmental conditions.

4. RGBT-VG Framework and Baseline

4.1. Unified Framework: RGBT-VG

We develop a unified multi-modal RGBT visual grounding framework, **RGBT-VG**, designed to systematically evaluate and extend existing grounding methods to multi-modal visual input settings. This framework is motivated by the limitations of prior VG pipelines, which are typically implemented for RGB-only data and follow heterogeneous training strategies. It provides a standardized, modality-agnostic, and extensible platform, enabling fair comparison across different architectures.

Specifically, RGBT-VG integrates a diverse set of representative 2D visual grounding models, including TransVG [6], MMCA [41], D-MDETR [29], CLIP-VG [33], HiVG [35], and OneRef [36]. We reformulate their input interfaces and feature fusion modules to operate under a consistent multimodal training paradigm. Within a single codebase, the framework supports RGB-only, TIR-only, and RGB-TIR inputs, allowing controlled evaluation of modality effects and systematic study of cross-modal feature adaptation. To ensure reproducible and comprehensive assessment, RGBT-VG unifies the data preprocessing pipeline, training routines, and evaluation metrics across all

models. This design allows researchers to directly compare model performance under complex real-world conditions. Furthermore, the unified framework provides the foundation for developing new multi-modal RGBT visual grounding models and serves as the infrastructure upon which we build our baseline method.

4.2. Baseline Method: RGBT-VGNet

Overall architecture. The architecture of multi-modal RGBT Visual Grounding baseline method (RGBT-VGNet) is illustrated in Figure 4. Given an RGB-TIR pair and a referring expression to localize the object described by the expression through integrating complementary cues. Specifically, RGBT-VGNet is built upon the CLIP model [28] and introduces two key components: ① Asymmetric Modality Adaptation (AMA) module that enables modality-adaptive visual feature learning, and ② Language-Aware Visual Synergy (LAVS) module that facilitates semantics-aware cross-modal interaction and fusion.

Formally, given an RGB image I_v , a TIR image I_t , and a referring expression $\mathbf{S} = \{\mathbf{s}_i\}_{i=1}^T$, the visual features at layer l (\mathbf{F}_v^l and \mathbf{F}_t^l) are extracted as:

$$\mathbf{f}_v^l = \begin{cases} \mathbb{E}_v^l(\mathbf{F}_v^{l-1}), & l > 1 \\ \mathbb{E}_v^l(\mathbf{I}_v), & l = 1 \end{cases}, \quad \mathbf{f}_t^l = \begin{cases} \mathbb{E}_v^l(\mathbf{F}_t^{l-1}), & l > 1 \\ \mathbb{E}_v^l(\mathbf{I}_t), & l = 1 \end{cases}, \quad (1)$$

where \mathbb{E}_v denotes the CLIP vision encoder with AMA module and $l \in \{1, \dots, n\}$ is the encoder layer index. The intermediate RGB and TIR features \mathbf{f}_v^l and \mathbf{f}_t^l are then refined by the LAVS module to produce the modality semantics-enhanced features \mathbf{F}_v^l and \mathbf{F}_t^l . The textual features are extracted as follows:

$$\mathbf{F}_s = \mathbb{E}_s(\mathbf{S}), \quad \mathbf{T}_s = \mathbb{P}_s(\mathbf{F}_s^n), \quad (2)$$

where \mathbb{E}_s denotes the CLIP text encoder, and \mathbb{P}_s is a linear projection that maps the last layer textual embeddings into the grounding space.

All CLIP encoders remain frozen to preserve the pre-trained language–vision alignment. The extracted representations are aligned and refined by the subsequent modules. The final input is composed by concatenating the projected RGB, TIR, and Text tokens with a learnable regression token [Reg], which is then fed into the vision–language transformer [35]. A lightweight regression head predicts the bounding box from the regression token:

$$\hat{\mathbf{B}} = \{\hat{x}, \hat{y}, \hat{w}, \hat{h}\}_i = \text{MLP}([\text{Reg}]). \quad (3)$$

① Asymmetric Modality Adaptation (AMA). The vision–language pre-trained models, such as CLIP, have exhibited strong performance on RGB domain. But the feature representations are biased toward the RGB modality used during pre-training, resulting in a huge modality gap when

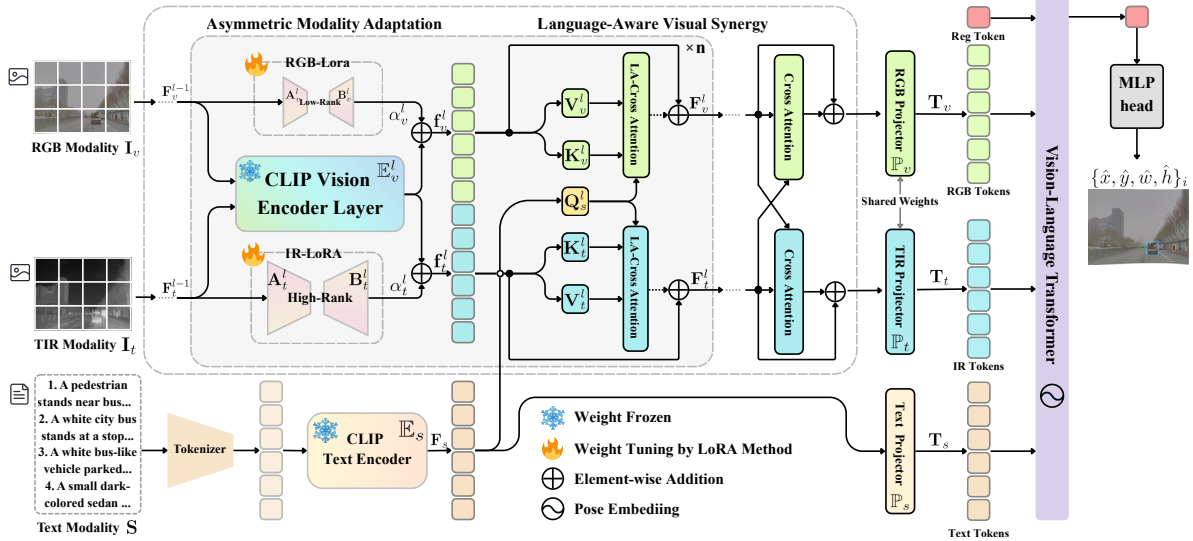


Figure 4. The architecture of the proposed multi-modal RGBT Visual Grounding baseline method (RGBT-VGNet).

extended to TIR modality. While LoRA-based [14] fine-tuning has been widely adopted to adapt frozen backbones to downstream tasks, applying identical LoRA configurations to different modalities overlooks their differences and the VLP models’ bias. To address this limitation, we introduce an asymmetric LoRA design that assigns different adaptation capacities to the two visual modalities. Specifically, we perform low-rank decomposition on the attention projection weights of each vision encoder layer l :

$$\mathbf{W}_v^l = \mathbf{W}_{\mathbb{E}_v}^l + \alpha_v^l \mathbf{A}_v^l \mathbf{B}_v^l, \quad \mathbf{W}_t^l = \mathbf{W}_{\mathbb{E}_v}^l + \alpha_t^l \mathbf{A}_t^l \mathbf{B}_t^l, \quad (4)$$

where $\mathbf{W}_{\mathbb{E}_v}^l$ is the frozen pre-trained weights of CLIP encoder, $\mathbf{A}_v^l, \mathbf{A}_t^l \in \mathbb{R}^{d \times r_v}, \mathbb{R}^{d \times r_t}$ and $\mathbf{B}_v^l, \mathbf{B}_t^l \in \mathbb{R}^{r_v \times d}, \mathbb{R}^{r_t \times d}$ are learnable low-rank matrices, and α^l is a scaling factor. We set asymmetric ranks $r_v \leq r_t$ for RGB and TIR modalities, allowing the TIR branch to learn richer modality-specific adaptations. We further adopt the hierarchical design [35] enabling progressive alignment from low-level structural to high-level semantic representations.

2 Language-Aware Visual Synergy. In the RGBT Visual Grounding task, the target described by the referring expression usually appears in both RGB and TIR images. Since grounding is inherently language-driven, we design a language-aware visual fusion module that uses textual features as semantic queries to guide multi-modal interaction, thereby enhancing localization precision. Given the encoder outputs \mathbf{f}_v^l and \mathbf{f}_t^l from layer l and the textual embedding \mathbf{F}_s , we first compute their Query–Key–Value projections and construct language-guided cross-modal attention:

$$\mathbf{A}_{\text{attn}_v}^l = \sigma \left(\frac{\mathbf{Q}_s^l (\mathbf{K}_v^l)^T}{\sqrt{d}} \right), \quad \mathbf{A}_{\text{attn}_t}^l = \sigma \left(\frac{\mathbf{Q}_s^l (\mathbf{K}_t^l)^T}{\sqrt{d}} \right), \quad (5)$$

where σ denotes the Softmax function and $\mathbf{A}_{\text{attn}_v}^l, \mathbf{A}_{\text{attn}_t}^l$

represent the attention matrices.

$$\begin{aligned} \mathbf{F}_v^l &= \mathbf{f}_v^l + (\mathbf{A}_{\text{attn}_v}^l)^T (\mathbf{A}_{\text{attn}_v}^l \mathbf{V}_v^l), \\ \mathbf{F}_t^l &= \mathbf{f}_t^l + (\mathbf{A}_{\text{attn}_t}^l)^T (\mathbf{A}_{\text{attn}_t}^l \mathbf{V}_t^l). \end{aligned} \quad (6)$$

Eq. 5 and 6 enable the textual semantics to guide the integration of visual cues from each modality. The textual semantics determining both which features should be fused and to what extent, meanwhile preserving feature dimensional consistency with left multiply by the transpose of $\mathbf{A}_{\text{attn}}^l$. After obtaining the text-queried visual features \mathbf{F}_v^l and \mathbf{F}_t^l , we apply cross-attention CA between the two visual modalities and feed into the:

$$\mathbf{T}_v^l = \mathbb{P}_v \left(\mathbf{F}_v^l + \text{CA}(\mathbf{F}_v^l, \mathbf{F}_t^l) \right), \quad \mathbf{T}_t^l = \mathbb{P}_t \left(\mathbf{F}_t^l + \text{CA}(\mathbf{F}_t^l, \mathbf{F}_v^l) \right) \quad (7)$$

where \mathbb{P}_v and \mathbb{P}_t denote the RGB and TIR modality linear projections, respectively, and mapping the outputs’ embeddings into a unified feature space for subsequent grounding.

5. Experiments

5.1. Experimental Setup

Implementation Details. Our methods are trained with 8 batch size, using AdamW as optimizer, learning rate 10e-4. Other models are trained with the settings following the default parameters specified in their original papers. All experiments are trained for totally 120 epochs with the same input image size (224 × 224), same data augmentation on NVIDIA RTX 4090 GPUs.

Evaluation Metrics. Following the previous visual grounding paper [5, 34], we adopt the **Acc@0.5** as the metrics, measuring the localization accuracy when the intersection-over-union (IoU) between the predicted and ground-truth bounding boxes exceeds 0.5. In addition, we report results sepa-

Table 4. Performance evaluation of current representative uni-modal visual grounding works and the baseline multi-modal RGBT visual grounding method on the RGBT-Ground benchmark. The “–” entries correspond to models that fail to produce stable bounding boxes. Complete evaluation results will be included in the supplementary materials.

Methods	Venue	Visual / Language Backbone	Visual Modality	RefFLIR					RefM ³ FD					RefMFAD				
				val	test	testA	testB	testC	val	test	testA	testB	testC	val	test	testA	testB	testC
a. Pretrained model zero-shot transfer setting:																		
CLIP-VG [33]	TMM’23	CLIP-B / CLIP-B	RGB	5.59	8.12	15.51	5.00	1.11	7.74	8.55	16.31	9.05	1.35	7.48	7.48	16.58	6.93	1.22
HiVG-B [35]	ACMMM’24	CLIP-B / CLIP-B		23.03	34.27	61.69	30.16	2.23	29.17	31.22	58.28	34.37	5.30	18.71	19.62	41.14	19.90	1.92
HiVG-L [35]	ACMMM’24	CLIP-L / CLIP-L		34.05	44.46	78.88	33.13	7.81	52.98	53.10	87.66	56.86	19.59	40.13	40.42	82.15	37.68	12.86
OneRef-B [36]	NeurIPS’24	BEIT3-B / BEIT3-B		32.89	41.46	77.68	31.56	3.55	33.93	39.65	74.11	48.63	3.19	29.70	30.05	70.63	28.14	2.86
OneRef-L [36]	NeurIPS’24	BEIT3-L / BEIT3-L		38.82	49.20	80.19	36.09	17.04	46.63	46.82	79.55	52.83	14.72	37.50	36.89	73.04	35.15	12.35
CLIP-VG [33]	TMM’23	CLIP-B / CLIP-B		4.77	8.03	14.92	6.41	0.61	2.38	6.59	9.33	11.15	0.76	4.54	4.26	9.49	4.04	5.49
HiVG-B [35]	ACMMM’24	CLIP-B / CLIP-B		10.86	12.10	20.64	15.94	0.81	7.74	11.49	18.34	18.19	0.97	6.29	7.36	17.97	6.44	0.51
HiVG-L [35]	ACMMM’24	CLIP-L / CLIP-L		18.26	23.80	43.56	24.06	0.00	24.40	28.89	55.36	36.47	2.92	23.73	23.11	56.33	20.39	2.82
OneRef-B [36]	NeurIPS’24	BEIT3-B / BEIT3-B		21.38	26.57	49.28	23.75	0.20	17.26	22.83	40.67	32.91	0.11	15.13	15.60	41.90	13.50	0.12
OneRef-L [36]	NeurIPS’24	BEIT3-L / BEIT3-L		21.55	27.00	46.42	26.56	3.65	23.21	23.65	38.15	33.55	4.17	17.52	17.81	41.14	16.39	2.43
b. Single source dataset training setting:																		
TransVG [6]	ICCV’21	RN50+DETR / BERT-B	RGB	50.74	42.16	62.25	34.89	19.76	39.29	40.08	63.42	46.03	15.10	52.27	51.94	82.64	49.35	31.06
CLIP-VG [33]	TMM’23	CLIP-B / CLIP-B		43.68	42.77	67.14	33.80	15.81	32.14	33.76	58.80	41.83	5.39	36.52	37.47	73.13	34.92	13.16
D-MDETR [29]	TPAMI’24	CLIP-B / CLIP-B		57.07	49.25	70.17	39.22	26.77	52.38	50.19	71.67	57.04	26.08	60.59	59.39	86.71	55.79	40.98
D-MDETR [29]	TPAMI’24	RN50+DETR / BERT-B		49.67	44.28	67.14	34.38	20.95	-	-	-	-	-	51.99	51.18	82.07	48.65	30.41
MMCA [41]	ACMMM’24	RN50+DETR / BERT-B		50.16	46.57	71.48	35.63	21.50	-	-	-	-	-	47.85	46.52	76.71	43.84	26.24
HiVG-B [35]	ACMMM’24	CLIP-B / CLIP-B		69.08	66.65	88.81	54.06	43.52	69.24	68.15	89.40	56.09	45.04	65.45	64.02	90.66	60.52	45.57
HiVG-L [35]	ACMMM’24	CLIP-L / CLIP-L		68.75	71.13	90.69	60.63	50.00	65.48	67.80	94.48	70.11	41.29	64.25	63.72	91.52	60.97	44.98
OneRef-B [36]	NeurIPS’24	BEIT3-B / BEIT3-B		63.82	61.69	84.73	52.34	35.90	66.07	66.66	94.64	70.93	39.07	62.34	60.61	90.76	57.63	40.86
OneRef-L [36]	NeurIPS’24	BEIT3-L / BEIT3-L		66.61	64.60	88.31	53.13	39.76	63.10	64.33	93.75	73.02	34.52	64.49	63.15	90.00	59.46	45.18
TransVG [6]	ICCV’21	RN50+DETR / BERT-B		49.92	42.63	62.37	35.67	21.18	45.83	47.54	69.72	55.58	22.51	52.79	52.33	83.92	49.84	31.37
CLIP-VG [33]	TMM’23	CLIP-B / CLIP-B	TIR	36.59	37.18	59.38	34.11	12.26	23.81	27.16	43.55	38.63	4.92	32.06	30.79	61.85	28.81	10.31
D-MDETR [29]	TPAMI’24	CLIP-B / CLIP-B		48.36	38.87	55.83	37.66	18.38	47.62	50.34	70.13	57.68	28.52	56.37	54.52	79.72	51.63	37.73
D-MDETR [29]	TPAMI’24	RN50+DETR / BERT-B		50.57	42.96	62.01	42.52	20.36	-	-	-	-	-	50.60	50.01	80.10	47.88	29.53
MMCA [41]	ACMMM’24	RN50+DETR / BERT-B		48.52	41.41	60.98	40.00	18.46	-	-	-	-	-	46.26	45.22	76.33	24.86	24.43
HiVG-B [35]	ACMMM’24	CLIP-B / CLIP-B		68.75	64.07	81.55	66.09	42.41	68.09	61.77	78.21	68.31	40.59	63.22	62.63	87.50	60.85	45.69
HiVG-L [35]	ACMMM’24	CLIP-L / CLIP-L		65.79	66.71	85.44	68.44	43.91	61.31	65.12	87.34	73.95	40.69	59.87	58.87	85.95	57.18	39.33
OneRef-B [36]	NeurIPS’24	BEIT3-B / BEIT3-B		62.01	60.00	80.55	60.00	35.80	60.12	65.10	87.74	73.03	41.02	58.60	57.95	86.46	55.71	38.67
OneRef-L [36]	NeurIPS’24	BEIT3-L / BEIT3-L		64.14	61.17	81.15	60.47	37.53	65.48	68.30	90.26	75.32	45.29	62.34	60.09	85.70	57.54	42.67
RGBT-VGNet	Baseline	CLIP-B / CLIP-B		73.68	72.65	91.31	67.19	52.22	73.21	74.34	94.72	81.93	53.63	67.83	66.63	91.16	64.07	49.76
			RGB+TIR															

rately for val, test, testA, testB, and testC subsets to evaluate model robustness under diverse conditions.

5.2. Evaluation on the RGBT-Ground Benchmark

Pretrained model zero-shot transfer setting. All models are evaluated by directly loading their pretrained weights without any fine-tuning on the RGBT-Ground dataset. As shown in Table 4, all methods exhibit low localization accuracy under both RGB and TIR modalities. This is primarily because the pretrained weights are trained on RefCOCO, ReferIt, and Flickr30K datasets, which contain limited scene complexity and lack of environmental diversity, making zero-shot transfer inherently difficult. Moreover, since these datasets are only RGB modality, the performance further degrades on the TIR modality, where the zero-shot results drop most drastically. Compared with the subsequently trained models, the zero-shot Acc@0.5 exhibits a substantial degradation of average 30% on RGB and 50% on TIR modality, respectively, demonstrating that effective cross-modal adaptation is necessary to achieve reliable multimodal RGBT visual grounding.

Single source dataset training setting. All models are trained under our unified framework with identical set-

tings. To combat the deterioration of RGB-modality visual grounding in low-light conditions and small objects, we introduce the TIR modality to provide illumination-invariant cues and thereby enhance overall robustness. In this setting, our RGBT-VGNet achieves highest performance across all three sub-datasets, benefiting from the complementary information offered by RGB-TIR fusion. Uni-modality visual grounding baselines such as HiVG [35] and OneRef [36] also show competitive results within their respective settings. In addition, all models trained on the target dataset exhibit superior improvements over their zero-shot versions, confirming the inherent difficulty of the RGBT-Ground benchmark.

Multi-modal RGBT visual grounding. As shown in Table 5, compared to the uni-modal visual grounding results (Table 4), multi-modal visual input consistently improves performance across all models, with an average improvement of approximately 10% in Acc@50. All models exhibit noticeable improvements on testB and testC, demonstrating the advantages of multimodal visual input under small objects and low light conditions. In particular, our RGBT-VGNet achieves the highest performance across all subsets, with Acc@50 metrics exceeding 91%, 64%, and 49%

Table 5. Performance comparison of multi-modal RGBT visual grounding methods on the RGBT-Ground benchmark. All results are obtained using our unified RGBT-VG framework for fair evaluation. ‘MV-Method’ denotes the multi-modal visual input extensions of the existing RGB-based visual grounding model.

Methods	Visual / Language Backbone	Modality	RefFLIR				RefM ³ FD				RefMFAD						
			val	test	testA	testB	testC	val	test	testA	testB	testC	val	test	testA	testB	testC
MV-TransVG	RN50+DETR / BERT-B CLIP-B / CLIP-B CLIP-B / CLIP-B RN50+DETR / BERT-B RN50+DETR / BERT-B CLIP-B / CLIP-B CLIP-L / CLIP-L BEIT3-B / BEIT3-B BEIT3-L / BEIT3-L CLIP-B / CLIP-B	RGB+TIR	54.44	46.06	68.62	40.31	21.10	45.83	48.04	70.29	55.3	22.89	53.18	53.84	83.54	51.14	33.84
MV-CLIP-VG			45.57	46.01	72.62	41.56	16.06	34.52	38.92	63.42	50.05	10.01	47.02	47.52	82.76	45.07	23.96
MV-D-MDETR			55.26	47.42	68.33	41.25	23.38	48.81	46.50	65.91	53.82	24.19	58.76	57.31	83.84	53.79	39.30
MV-D-MDETR			55.01	47.84	68.10	43.77	24.52	44.64	45.62	67.23	53.88	21.81	54.73	54.13	82.89	52.00	34.24
MV-MMCA			54.93	48.97	72.43	42.34	22.62	46.43	47.83	72.16	56.76	20.45	53.62	54.41	84.41	51.47	34.16
MV-HiVG-B			75.33	69.20	85.80	66.72	50.20	69.64	72.35	93.99	79.43	49.40	67.07	67.04	91.01	64.52	51.53
MV-HiVG-L			71.05	72.50	91.07	70.17	51.16	63.16	68.67	89.52	63.28	44.74	61.78	61.31	88.38	58.85	42.36
MV-OneRef-B			63.82	62.05	86.19	57.34	35.43	62.50	63.98	89.20	69.34	37.93	61.62	59.97	89.25	56.85	41.58
MV-OneRef-L			66.61	60.89	84.01	53.75	35.09	67.26	69.70	92.78	75.14	46.27	64.57	62.73	88.99	59.42	45.25
RGBT-VGNet			<u>73.68</u>	72.65	91.31	<u>67.19</u>	52.22	73.21	74.34	94.72	81.93	53.63	67.83	<u>66.63</u>	91.16	64.57	<u>49.76</u>



1. A silver sedan parked on a wet plaza in front of a large building. 2. A person in a black and white striped sweater walks across the wet plaza. 3. A yellow bus with a rectangular shape and visible windows is parked on the wet pavement in front of a building.



1. A pedestrian stands near bus shelters along a city street under overcast skies. 2. A white city bus stands at a stop near the right side of the road, surrounded by trees under overcast skies. 3. A white bus-like vehicle parked at a designated stop along the road.



1. Black bicycle with rider pedaling along the street. 2. A small, light-colored car is parked along the street near the sidewalk. 3. Person riding a bicycle, wearing dark clothing and a helmet, positioned centrally on the street.

Figure 5. Qualitative comparison of multi-modal RGBT visual grounding results on RGBT-Ground. The three rows correspond to RefM³FD, RefMFAD, and RefFLIR sub-datasets, respectively. Bounding box colors match the description below. Each column shows a different visual grounding method, stressing differences across methods under diverse illumination, weather, object size, and occlusion.

on testA, testB, and testC, respectively, further validating its robustness and generalization under diverse lighting and object-size conditions. **More evaluation results will be included in the Appendix.**

5.3. Qualitative Comparisons and Analysis

The qualitative comparison of multi-modal RGBT visual grounding models on the RGBT-Ground benchmark is shown in Figure 5. The objects are in various real-world conditions, including post-rain, foggy, and sunny weather, which presents challenges for models with different lighting, visibility, and object sizes. All results are evaluated using our framework adapted to the RGB–Thermal modality. The results reveal that uni-modal visual grounding methods struggle with small or distant targets, often producing overly large or inaccurate boxes. In contrast, RGBT-VGNet consistently delivers precise and semantically consistent detections for humans and vehicles, effectively leveraging complementary cues from RGB and Thermal modalities under textual guidance. This demonstrates its robustness and generalization in various complex scenarios.

6. Conclusion

In this work, we introduced RGBT-Ground, the first large-scale RGB–Thermal visual grounding benchmark tailored for complex real-world scenarios. Featuring diverse scenes, challenging illumination and weather conditions, as well as a high proportion of small and occluded objects, RGBT-Ground offers a significantly more comprehensive testbed for assessing model robustness. To accommodate multi-modal visual inputs, we developed a unified framework that extends existing uni-modal visual grounding methods to the RGB–Thermal setting. Building upon this framework, we proposed RGBT-VGNet, an effective baseline that exploits the complementary strengths of RGB and thermal infrared cues for reliable target localization. Extensive experiments across various sub-datasets and evaluation settings reveal the limitations of current uni-modal visual grounding models under adverse conditions and underscore the advantages of multimodal input. All resources will be publicly released to promote future research on robust visual grounding in complex real-world environments.

References

[1] Jinze Bai, Shuai Bai, Shusheng Yang, Shijie Wang, Sinan Tan, Peng Wang, Junyang Lin, Chang Zhou, and Jingren Zhou. Qwen-vl: A versatile vision-language model for understanding, localization, text reading, and beyond, 2023. 5

[2] Yen-Chun Chen, Linjie Li, Licheng Yu, Ahmed El Kholy, Faisal Ahmed, Zhe Gan, Yu Cheng, and Jingjing Liu. Uniter: Universal image-text representation learning. In *ECCV*, pages 104–120. Springer, 2020. 2

[3] Zhenfang Chen, Peng Wang, Lin Ma, Kwan-Yee K Wong, and Qi Wu. Cops-ref: A new dataset and task on compositional referring expression comprehension. In *CVPR*, pages 10086–10095, 2020. 1

[4] Zhenyu Chen, Ronghang Hu, Xinlei Chen, Matthias Nießner, and Angel X Chang. Unit3d: A unified transformer for 3d dense captioning and visual grounding. In *ICCV*, pages 18109–18119, 2023. 3

[5] Zhihong Chen, Ruifei Zhang, Yibing Song, Xiang Wan, and Guanbin Li. Advancing visual grounding with scene knowledge: Benchmark and method. In *CVPR*, pages 15039–15049, 2023. 6

[6] Jiajun Deng, Zhengyuan Yang, Tianlang Chen, Wengang Zhou, and Houqiang Li. Transvg: End-to-end visual grounding with transformers. In *ICCV*, pages 1769–1779, 2021. 2, 5, 7, 12, 22, 23, 24, 25, 26, 27

[7] Jacob Devlin, Ming-Wei Chang, Kenton Lee, and Kristina Toutanova. Bert: Pre-training of deep bidirectional transformers for language understanding. In *Proceedings of the 2019 conference of the North American chapter of the association for computational linguistics: human language technologies, volume 1 (long and short papers)*, pages 4171–4186, 2019. 2

[8] Dinh Phat Do, Taehoon Kim, Jaemin Na, Jiwon Kim, Keonho Lee, Kyunghwan Cho, and Wonjun Hwang. D3t: Distinctive dual-domain teacher zigzagging across rgb-thermal gap for domain-adaptive object detection. In *CVPR*, pages 23313–23322, 2024. 3

[9] Alexey Dosovitskiy. An image is worth 16x16 words: Transformers for image recognition at scale. *arXiv preprint arXiv:2010.11929*, 2020. 2

[10] Zhe Gan, Yen-Chun Chen, Linjie Li, Chen Zhu, Yu Cheng, and Jingjing Liu. Large-scale adversarial training for vision-and-language representation learning. *NeurIPS*, 33:6616–6628, 2020. 2

[11] Chen Gao, Jinyu Chen, Si Liu, Luting Wang, Qiong Zhang, and Qi Wu. Room-and-object aware knowledge reasoning for remote embodied referring expression. In *CVPR*, pages 3064–3073, 2021. 1

[12] Michael Grubinger, Paul Clough, Henning Müller, and Thomas Deselaers. The iapt tc-12 benchmark: A new evaluation resource for visual information systems. In *International workshop ontoImage*, 2006. 3

[13] Kaiming He, Xiangyu Zhang, Shaoqing Ren, and Jian Sun. Deep residual learning for image recognition. In *Proceedings of the IEEE conference on computer vision and pattern recognition*, pages 770–778, 2016. 2

[14] Edward J Hu, Yelong Shen, Phillip Wallis, Zeyuan Allen-Zhu, Yuanzhi Li, Shean Wang, Lu Wang, Weizhu Chen, et al. Lora: Low-rank adaptation of large language models. *ICLR*, 1(2):3, 2022. 6

[15] Ke Hu, Yudong He, Yuan Li, Jiayu Zhao, Song Chen, and Yi Kang. Ei 2 det: Edge-guided illumination-aware interactive learning for visible-infrared object detection. *TCSVT*, 2025. 3

[16] Yutao Hu, Qixiong Wang, Wenqi Shao, Enze Xie, Zhenguo Li, Jungong Han, and Ping Luo. Beyond one-to-one: Rethinking the referring image segmentation. In *ICCV*, pages 4067–4077, 2023. 1

[17] Sahar Kazemzadeh, Vicente Ordonez, Mark Matten, and Tamara Berg. Referitgame: Referring to objects in photographs of natural scenes. In *EMNLP*, pages 787–798, 2014. 1, 3

[18] Chenliang Li, Haiyang Xu, Junfeng Tian, Wei Wang, Ming Yan, Bin Bi, Jiabo Ye, He Chen, Guohai Xu, Zheng Cao, et al. mplug: Effective and efficient vision-language learning by cross-modal skip-connections. In *EMNLP*, pages 7241–7259, 2022. 2

[19] Gongyang Li, Yike Wang, Zhi Liu, Xinpeng Zhang, and Dan Zeng. Rgb-t semantic segmentation with location, activation, and sharpening. *TCSVT*, 33(3):1223–1235, 2022. 3

[20] Tsung-Yi Lin, Michael Maire, Serge Belongie, James Hays, Pietro Perona, Deva Ramanan, Piotr Dollár, and C Lawrence Zitnick. Microsoft coco: Common objects in context. In *ECCV*, pages 740–755. Springer, 2014. 3

[21] Chang Liu, Henghui Ding, and Xudong Jiang. Gres: Generalized referring expression segmentation. In *CVPR*, pages 23592–23601, 2023. 1

[22] Haolin Liu, Anran Lin, Xiaoguang Han, Lei Yang, Yizhou Yu, and Shuguang Cui. Refer-it-in-rgbd: A bottom-up approach for 3d visual grounding in rgbd images. In *CVPR*, pages 6032–6041, 2021. 3

[23] Haotian Liu, Chunyuan Li, Qingyang Wu, and Yong Jae Lee. Visual instruction tuning. *NeurIPS*, 36:34892–34916, 2023. 1

[24] Jinyuan Liu, Xin Fan, Zhanbo Huang, Guanyao Wu, Risheng Liu, Wei Zhong, and Zhongxuan Luo. Target-aware dual adversarial learning and a multi-scenario multi-modality benchmark to fuse infrared and visible for object detection. In *CVPR*, pages 5802–5811, 2022. 3

[25] Taiki Miyanishi, Daichi Azuma, Shuhei Kurita, and Motoaki Kawanabe. Cross3dvg: Cross-dataset 3d visual grounding on different rgb-d scans. In *2024 International Conference on 3D Vision (3DV)*, pages 717–727. IEEE, 2024. 3

[26] Varun K Nagaraja, Vlad I Morariu, and Larry S Davis. Modeling context between objects for referring expression understanding. In *ECCV*, pages 792–807. Springer, 2016. 1, 3

[27] Bryan A Plummer, Liwei Wang, Chris M Cervantes, Juan C Caicedo, Julia Hockenmaier, and Svetlana Lazebnik. Flickr30k entities: Collecting region-to-phrase correspondences for richer image-to-sentence models. In *ICCV*, pages 2641–2649, 2015. 1, 3

[28] Alec Radford, Jong Wook Kim, Chris Hallacy, Aditya Ramesh, Gabriel Goh, Sandhini Agarwal, Girish Sastry,

Amanda Askell, Pamela Mishkin, Jack Clark, et al. Learning transferable visual models from natural language supervision. In *ICLR*, pages 8748–8763. PMLR, 2021. [1](#), [5](#)

[29] Fengyuan Shi, Ruopeng Gao, Weilin Huang, and Limin Wang. Dynamic mdetr: A dynamic multimodal transformer decoder for visual grounding. *IEEE Transactions on Pattern Analysis and Machine Intelligence*, 46(2):1181–1198, 2023. [2](#), [5](#), [7](#), [12](#), [22](#), [23](#), [24](#), [25](#), [26](#), [27](#)

[30] Ashish Vaswani, Noam Shazeer, Niki Parmar, Jakob Uszkoreit, Llion Jones, Aidan N Gomez, Łukasz Kaiser, and Illia Polosukhin. Attention is all you need. *NeurIPS*, 30, 2017. [2](#)

[31] Peng Wang, An Yang, Rui Men, Junyang Lin, Shuai Bai, Zhikang Li, Jianxin Ma, Chang Zhou, Jingren Zhou, and Hongxia Yang. Ofa: Unifying architectures, tasks, and modalities through a simple sequence-to-sequence learning framework. In *ICLR*, pages 23318–23340. PMLR, 2022. [2](#)

[32] Wenhui Wang, Hangbo Bao, Li Dong, Johan Bjorck, Zhiliang Peng, Qiang Liu, Kriti Aggarwal, Owais Khan Mohammed, Saksham Singh, Subhajit Som, et al. Image as a foreign language: Beit pretraining for vision and vision-language tasks. In *CVPR*, pages 19175–19186, 2023. [1](#)

[33] Linhui Xiao, Xiaoshan Yang, Fang Peng, Ming Yan, Yaowei Wang, and Changsheng Xu. Clip-vg: Self-paced curriculum adapting of clip for visual grounding. *TMM*, 26:4334–4347, 2023. [2](#), [5](#), [7](#), [12](#), [22](#), [23](#), [24](#), [25](#), [26](#), [27](#)

[34] Linhui Xiao, Xiaoshan Yang, Xiangyuan Lan, Yaowei Wang, and Changsheng Xu. Towards visual grounding: A survey. *arXiv preprint arXiv:2412.20206*, 2024. [6](#)

[35] Linhui Xiao, Xiaoshan Yang, Fang Peng, Yaowei Wang, and Changsheng Xu. Hivg: Hierarchical multimodal fine-grained modulation for visual grounding. In *Proceedings of the 32nd ACM International Conference on Multimedia*, pages 5460–5469, 2024. [2](#), [5](#), [6](#), [7](#), [12](#), [22](#), [23](#), [24](#), [25](#), [26](#), [27](#)

[36] Linhui Xiao, Xiaoshan Yang, Fang Peng, Yaowei Wang, and Changsheng Xu. Oneref: Unified one-tower expression grounding and segmentation with mask referring modeling. *NeurIPS*, 37:139854–139885, 2024. [5](#), [7](#), [12](#), [22](#), [23](#), [24](#), [25](#), [26](#), [27](#)

[37] Chi Xie, Zhao Zhang, Yixuan Wu, Feng Zhu, Rui Zhao, and Shuang Liang. Described object detection: Liberating object detection with flexible expressions. *NeurIPS*, 36:79095–79107, 2023. [1](#)

[38] Yunqiu Xu, Linchao Zhu, and Yi Yang. Mc-bench: A benchmark for multi-context visual grounding in the era of mllms. In *ICCV*, pages 17675–17687, 2025. [1](#)

[39] Zhengyuan Yang, Tianlang Chen, Liwei Wang, and Jiebo Luo. Improving one-stage visual grounding by recursive sub-query construction. In *ECCV*, pages 387–404. Springer, 2020. [2](#)

[40] Zhengyuan Yang, Zhe Gan, Jianfeng Wang, Xiaowei Hu, Faisal Ahmed, Zicheng Liu, Yumao Lu, and Lijuan Wang. Unitab: Unifying text and box outputs for grounded vision-language modeling. In *ECCV*, pages 521–539. Springer, 2022. [2](#)

[41] Ruilin Yao, Shengwu Xiong, Yichen Zhao, and Yi Rong. Visual grounding with multi-modal conditional adaptation. In *Proceedings of the 32nd ACM International Conference on Multimedia*, pages 3877–3886, 2024. [5](#), [7](#), [12](#), [22](#), [23](#), [24](#), [25](#), [26](#), [27](#)

[42] Jiabo Ye, Junfeng Tian, Ming Yan, Xiaoshan Yang, Xuwu Wang, Ji Zhang, Liang He, and Xin Lin. Shifting more attention to visual backbone: Query-modulated refinement networks for end-to-end visual grounding. In *CVPR*, pages 15502–15512, 2022. [2](#)

[43] Licheng Yu, Patrick Poirson, Shan Yang, Alexander C Berg, and Tamara L Berg. Modeling context in referring expressions. In *ECCV*, pages 69–85. Springer, 2016. [1](#), [3](#)

[44] Maoxun Yuan and Xingxing Wei. C²former: Calibrated and complementary transformer for rgb-infrared object detection. *TGRS*, 62:1–12, 2024. [3](#)

[45] Maoxun Yuan, Yinyan Wang, and Xingxing Wei. Translation, scale and rotation: Cross-modal alignment meets rgb-infrared vehicle detection. In *ECCV*, pages 509–525. Springer, 2022. [1](#)

[46] Maoxun Yuan, Xiaorong Shi, Nan Wang, Yinyan Wang, and Xingxing Wei. Improving rgb-infrared object detection with cascade alignment-guided transformer. *Information Fusion*, 105:102246, 2024. [1](#)

[47] Maoxun Yuan, Bo Cui, Tianyi Zhao, Jiayi Wang, Shan Fu, Xue Yang, and Xingxing Wei. Unirgb-ir: A unified framework for visible-infrared semantic tasks via adapter tuning. In *ACM MM*, pages 2409–2418, 2025. [3](#)

[48] Heng Zhang, Elisa Fromont, Sébastien Lefevre, and Bruno Avignon. Multispectral fusion for object detection with cyclic fuse-and-refine blocks. In *ICIP*, pages 276–280. IEEE, 2020. [3](#)

[49] Qiang Zhang, Shenlu Zhao, Yongjiang Luo, Dingwen Zhang, Nianchang Huang, and Jungong Han. Abmdrnet: Adaptive-weighted bi-directional modality difference reduction network for rgb-t semantic segmentation. In *CVPR*, pages 2633–2642, 2021. [3](#)

[50] Tianyi Zhao, Maoxun Yuan, Feng Jiang, Nan Wang, and Xingxing Wei. Removal then selection: A coarse-to-fine fusion perspective for rgb-infrared object detection. *arXiv e-prints*, pages arXiv–2401, 2024. [3](#)

[51] Tianyi Zhao, Boyang Liu, Yanglei Gao, Yiming Sun, Maoxun Yuan, and Xingxing Wei. Rethinking multi-modal object detection from the perspective of mono-modality feature learning. In *ICCV*, pages 6364–6373, 2025. [3](#)

Appendix

A More Evaluation Results on RGBT-Ground	12
A.1. Evaluation on More Sub-datasets	12
A.2 Evaluation Methods	12
A.3 Results on Scene-Type Subsets (13 categories)	12
A.4 Results on Weather Subsets (4 categories)	13
A.5 Results on Illumination Subsets (4 categories)	13
A.6 Results on Object Size Subsets (2 categories)	14
A.7 Results on Occlusion Subsets (2 categories)	15
A.8 Summary	15
B More Qualitative Comparison Experiments	16
C Ablation on RGBT-VGNet Components	18
D Complete Data Annotation Process	19
D.1. Scene and Weather Annotation Prompt	19
D.2 Lighting Annotation Prompt	19
D.3 Object-Level Annotation Prompts and Rules	20
E Potential Applications of the RGBT-Ground	20
E.1. Referring Expression Segmentation (RES)	20
E.2. Visual Question Answering (VQA)	21
E.3. Cross-Modal Retrieval	21

A. More Evaluation Results on RGBT-Ground

A.1. Evaluation on More Sub-datasets.

To complement the results presented in the manuscript, we provide additional evaluations across all fine-grained subsets included in the proposed RGBT-Ground benchmark. These subsets correspond to the multi-level annotations described in the dataset:

- **13 Scene Types:** Urban (UB), Intersection (IT), Residential (RS), Suburban (SU), Highway (HW), Campus (CP), Bridge (BG), Parking Lot (PL), Rural (RR), Tunnel (TN), Market/Shopping Area (MK), Waterfront (WF), Industrial (ID)
- **4 Weather Conditions:** Cloudy (CY), Foggy (FY), Rainy (RY), Sunny (SY)
- **4 Illumination Conditions:** Strong Light (SL), Normal Light (NL), Weak Light (WL), Very Weak Light (VL)
- **2 Occlusion Levels:** No-or-Partial (PO), Heavy (HO)
- **2 Object Sizes:** Normal Size (NS), Small Size (SS)

A.2. Evaluation Methods.

All experiments follow the unified **RGBT-VG** framework introduced in the manuscript, using the same image resolution 224×224 . We evaluate the same set of representative RGB-only, TIR-only, and RGB-TIR multi-modal grounding models listed in Table 4 and Table 5 of the manuscript, including:

- TransVG [6]
- CLIP-VG [33]
- D-MDETR [29]
- MMCA [41]
- HiVG-B / HiVG-L [35]
- OneRef-B / OneRef-L [36]
- MV-methods (multi-modal visual input method adapted from RGB-only method)
- RGBT-VGNet

Performance is measured using Acc@0.5, consistent with the manuscript.

A.3. Results on Scene-Type Subsets (13 categories)

To analyze the impact of scene semantics on grounding performance, we evaluate all methods across the 13 scene categories in RGBT-Ground. The scene-level Acc@0.5 results on the three sub-datasets RefFLIR, RefM³FD, and RefMFAD are reported in Tables 8, 9, and 10, respectively. These tables follow the same organization as the main paper, and include pretrained zero-shot transfer, single-source training, and multi-modal RGB+TIR settings. Below we summarize the main observations.

Diversity of scene semantics. The 13 scene types cover a wide range of realistic environments. Different scenes exhibit very different combinations of lighting conditions, background clutter, object density, and typical viewing an-

gles. The clear variation in performance across columns in Tables 8–10 confirms that scene semantics is an important factor that stresses different aspects of visual grounding.

RGB vs. RGB-TIR across scenes. A consistent trend across all three sub-datasets is that RGB+TIR models achieve clear gains over their RGB-only and TIR-only counterparts in the more challenging scenes:

- In **rural (RR)** and **tunnel (TN)** scenes, where illumination is often non-uniform and texture is weak, RGB-only models show a noticeable drop, while RGB+TIR variants maintain much higher accuracy. This indicates that thermal cues compensate for the lack of reliable RGB appearance in these environments.
- In **parking lot (PL)** and **market (MK)** scenes, objects are densely packed and frequently occlude each other. RGB+TIR models improve over single-modality baselines in nearly all cases, suggesting that thermal signals help distinguish the correct target among many visually similar distractors.
- In **highway (HW)** and bridge scenes (BG), backgrounds are relatively simple and objects are often far away. RGB-only models are already competitive, yet RGB+TIR fusion still brings incremental gains, especially for distant or partially visible targets.

Comparison across training settings and methods. When comparing different architectures and training strategy, we observe:

- **Zero-shot transfer.** In the pretrained zero-shot setting, CLIP-based and BEiT3-based RGB models provide a reasonable starting point, but their performance varies significantly across scenes. Zero-shot TIR models generally lag behind their RGB counterparts, reflecting the domain gap between the pretraining data and thermal imagery. This highlights the importance of task-specific fine-tuning.
- **Single-source training.** After training on a single RGBT-Ground sub-dataset, both RGB-only and TIR-only models improve substantially, but they remain sensitive to scene changes: methods relying heavily on high-level RGB semantics still degrade in low-texture or low-light scenes such as RR and TN, while TIR-only models struggle in scenes where temperature contrast is weak.
- **Multimodal extensions (MV-*) vs. single-modality baselines.** The MV-* variants, which extend existing RGB architectures to RGB+TIR input, consistently narrow the performance gap across almost all scene types and datasets. In particular, they show clear advantages in RR, TN, PL, and MK, confirming the benefit of exploiting complementary modalities in challenging scenes.
- **RGBT-VGNet.** The proposed RGBT-VGNet achieves the best or second-best performance in almost all scene types on RefFLIR, RefM³FD, and RefMFAD. Its gains over other RGB+TIR models are most notable in difficult scenes such as RR, TN, PL, and MK, where both

illumination and layout are complex. This suggests that the combination of AMA and LAVS enables more effective cross-modal adaptation and language-aware fusion, leading to robust scene-level performance across diverse environments.

Benchmark-level observations. From a benchmark perspective, the scene-wise results reveal several useful properties of RGBT-Ground:

- **Modality sensitivity is scene-dependent.** The performance gaps between RGB-only, TIR-only, and RGB+TIR models are highly scene-specific: scenes dominated by illumination or occlusion issues benefit more from thermal information, whereas structurally simple scenes are largely saturated by RGB cues. This makes RGBT-Ground a suitable testbed for studying when additional sensing modalities are most valuable.
- **Ranking robustness across datasets.** Despite the differences between RefFLIR, RefM³FD, and RefMFAD, the relative ranking of methods is largely consistent across the three sub-datasets for a given scene type. This suggests that the benchmark provides stable measurements of model capability rather than dataset-specific artifacts, and can therefore be used to fairly compare future multi-modal grounding approaches.

A.4. Results on Weather Subsets (4 categories)

We further evaluate the robustness of all methods under four weather conditions. The detailed Acc@0.5 results on are summarized in Table 11, which follows the same organization as the scene-wise tables.

Impact of adverse weather. Adverse weather significantly affects the visibility and appearance of objects in RGB images (as shown in Figure 6 7 8 and 9), and this trend is clearly reflected in the table:

- **Foggy (FY)** are consistently the most challenging conditions. In both zero-shot and single-source, RGB-only models show a clear drop in accuracy from SY to FY across all three sub-datasets. The reduced contrast, veiling glare, and scattering effects in FY/RY degrade high-level RGB semantics and make it difficult to precisely localize targets, especially at medium and long ranges.
- **Cloudy (CY)** scenes are less extreme: RGB-only models exhibit moderate drops compared with SY but remain relatively stable, as illumination is still sufficient and texture is largely preserved.

In contrast, the thermal modality is much less sensitive to these appearance changes, since it captures emitted or reflected infrared radiation rather than visible light. TIR-only and RGB+TIR models therefore maintain more stable performance under FY and RY, particularly in the single-source and multi-modal rows of Table 11.

Advantages of multi-modal fusion. Across all three sub-datasets, multi-modal models (MV-* variants and RGBT-

VGNet) show clear advantages over their single-modality counterparts:

- The performance gap between RGB-only and RGB+TIR models is most pronounced in **FY** columns, where visible contrast is heavily reduced while thermal responses remain informative.
- Gains are also evident in **RY** columns, suggesting that RGB+TIR fusion compensates for rain streaks, reflections, and motion blur that frequently degrade RGB quality.
- Under **CY** and **SY**, RGB-only models are already strong, but RGB+TIR still brings incremental improvements, indicating that thermal information can provide complementary cues even in relatively benign weather.

Performance of RGBT-VGNet. Our RGBT-VGNet attains the highest or second-highest accuracy in almost all weather conditions and datasets. In particular, its improvements over other RGB+TIR models are most visible in FY and RY, where the combination of AMA and LAVS yields stronger robustness to visibility degradation and background clutter. These results support the conclusion that carefully designed cross-modal interaction and language-aware fusion are especially beneficial when weather conditions significantly alter RGB appearance.

Benchmark-level observations. From a benchmark perspective, the weather-wise results reveal several useful characteristics of RGBT-Ground:

- **Consistent difficulty ordering.** For almost all models and training settings, SY > CY > (FY, RY) in terms of accuracy, indicating that the four subsets form a meaningful and stable difficulty spectrum for evaluating robustness to weather.
- **Scene–weather interaction.** The benefit of TIR is amplified in adverse weather, particularly when combined with challenging scenes (e.g., rural roads or crowded markets). This makes the benchmark suitable for studying how environmental factors and sensing modalities jointly affect grounding performance.
- **Cross-dataset stability.** The relative ranking of methods under each weather condition is largely consistent across RefFLIR, RefM³FD, and RefMFAD, suggesting that the weather annotations provide reliable signals rather than dataset-specific artifacts and can thus serve as a robust basis for future method comparison.

A.5. Results on Illumination Subsets (4 categories)

The illumination subsets complement the TestB (low-light) evaluation in the main manuscript by providing four explicit illumination levels. The Acc@0.5 results on RefFLIR, RefM³FD, and RefMFAD are reported in Table 12, using the same organization as the scene-wise and weather-wise tables.

Illumination sensitivity of RGB-only models.

- In **SL** and **NL** conditions, RGB-only methods achieve relatively high performance on all three sub-datasets. In these regimes, appearance cues, color contrast, and contextual details are clearly visible, and high-level RGB semantics remain reliable.
- As illumination decreases from **NL** to **WL** and further to **VL**, all RGB-only baselines exhibit a sharp accuracy drop. This trend is consistent in both the zero-shot and single-source settings in Table 12. Low-light images contain stronger noise, reduced dynamic range, and missing color information, which substantially impairs the ability of RGB-only models to localize the referred objects, especially at medium and long distances.

Characteristics of TIR-only models. Thermal-only models show a different pattern:

- Their performance is generally lower than RGB-only methods in **SL** and **NL**, where visible textures and colors provide rich discriminative cues that are not fully captured by TIR.
- However, as illumination weakens, TIR-only models degrade much more slowly than RGB-only ones, and in several **VL** cases they become comparable or superior to RGB-only models, reflecting the illumination invariance of thermal sensing.

Advantages of RGB+TIR fusion. Across all three sub-datasets, multi-modal RGB+TIR models (MV-* variants and RGBT-VGNet) provide the best balance between semantic richness and robustness to illumination changes:

- In **SL/NL**, RGB+TIR models perform at least on par with the best RGB-only models, indicating that fusion does not harm performance in well-lit conditions.
- In **WL/VL**, RGB+TIR models clearly outperform both RGB-only and TIR-only baselines, confirming that the two modalities provide complementary information: RGB offers high-level semantics when usable, whereas TIR supplies stable structural cues when RGB deteriorates.

Performance of RGBT-VGNet. The proposed RGBT-VGNet achieves the highest or second-highest accuracy in almost all illumination conditions and datasets. Its advantage is particularly pronounced in the **VL** columns of Table 12, where most RGB-only models collapse. The combination of AMA and LAVS allows RGBT-VGNet to rely more on TIR features when RGB becomes unreliable, while still exploiting RGB details under **SL** and **NL**. This leads to consistently strong performance across the entire illumination spectrum.

Benchmark-level observations. From a benchmark perspective, the illumination-wise results highlight several useful properties of RGBT-Ground:

- **Clear difficulty progression.** For nearly all methods, accuracy follows the ordering $SL \approx NL > WL > VL$, forming a stable difficulty ladder for evaluating robustness to

illumination degradation.

- **Modality roles are illumination-dependent.** RGB dominates in **SL/NL**, TIR becomes increasingly important in **WL/VL**, and RGB+TIR fusion yields the best overall trade-off. This makes the benchmark well-suited for studying when and how additional modalities should be exploited.
- **Consistent method ranking across datasets.** The relative ranking of models at each illumination level is largely consistent across RefFLIR, RefM³FD, and RefMFAD, suggesting that the illumination labels provide reliable, dataset-agnostic signals and can serve as a solid basis for future comparisons.

A.6. Results on Object Size Subsets (2 categories)

Although TestC in the main manuscript already focuses on small objects, here we report the full evaluation on Normal-Size (NS) and Small-Size (SS) subsets for RefFLIR, RefM³FD, and RefMFAD in Table 13.

Challenges of small objects.

- **Small-size (SS)** targets remain the most challenging across all datasets and methods. Their limited pixel footprint and frequent partial occlusions make it difficult to extract discriminative visual features, and precise grounding requires accurate localization in very small regions.
- RGB-only models exhibit substantial performance degradation when moving from NS to SS, indicating that simply scaling model capacity or backbone strength is not sufficient to solve the small-object problem.

Effect of RGB-TIR fusion and RGBT-VGNet.

- RGB-TIR fusion generally yields consistent improvements on both NS and SS subsets. The gains are especially notable on SS, where thermal cues help highlight pedestrians and vehicles that are only weakly visible in RGB, particularly in cluttered or low-light environments.
- Multimodal MV-* baselines reduce the NS \rightarrow SS performance drop compared with single-modality models, demonstrating that complementary modalities are beneficial for tiny targets.
- **RGBT-VGNet** achieves the best or second-best performance on NS and SS across the three sub-datasets, with the largest margins typically observed on the SS subset. This confirms that the proposed **AMA** and **LAVS** modules effectively capture cross-modal cues and focus attention on small, linguistically referred instances.

Benchmark-level observations. The size-wise results further characterize RGBT-Ground as a benchmark:

- For nearly all methods, NS $>$ SS in accuracy, forming a clear and stable difficulty hierarchy with respect to object scale.
- The benefit of RGB+TIR fusion is more pronounced on SS than on NS, showing that multi-modal information is particularly valuable when visual evidence in a single

modality is extremely limited.

- Consistent trends across RefFLIR, RefM³FD, and RefMFAD indicate that the size annotations capture a general challenge rather than dataset-specific bias, providing a solid basis for evaluating future methods targeting small-object grounding.

A.7. Results on Occlusion Subsets (2 categories)

To explicitly examine the influence of object occlusion, we report Acc@0.5 on the No-or-Partial Occlusion (PO) and Heavy Occlusion (HO) subsets for each sub-dataset in Table 13.

Effect of occlusion on single-modality models.

- Under the **PO** subset, most methods obtain relatively high and stable performance, since the referred objects are fully visible or only lightly occluded. In this regime, a strong semantic alignment between text and RGB appearance cues is usually sufficient for accurate grounding.
- Under the **HO** subset, all single-modality models suffer a noticeable drop, with RGB-only models being affected the most. When large portions of the target are occluded by other objects or scene structures, RGB appearance becomes highly ambiguous and models often confuse the target with nearby distractors.
- TIR-only models are slightly more robust than RGB-only models in HO for some cases, as thermal signals can still capture coarse shape or heat signatures. However, the lack of fine-grained semantics limits their overall accuracy.

Benefits of thermal cues and multi-modal fusion.

- Thermal cues provide complementary information that remains visible even when RGB texture is severely occluded or visually similar to the background. This is reflected by the fact that RGB+TIR models exhibit significantly smaller performance drops from PO to HO compared with RGB-only baselines on all three sub-datasets.
- Multimodal extensions (MV-* variants) consistently improve over their single-modality counterparts in both PO and HO subsets, indicating that simple fusion strategies already help the model disambiguate occluded targets.
- **RGBT-VGNet** further reduces the PO→HO gap and achieves the highest or second-highest accuracy in most occlusion settings. Its language-aware fusion (LAVS) allows the model to exploit relational phrases (e.g., “behind the truck”, “next to the bike”) to select the correct RGB-TIR regions, which is particularly important under heavy occlusion.

Benchmark-level observations. From a benchmark perspective, the occlusion-wise results show that:

- HO is consistently more difficult than PO for all methods and training settings, providing a clear and stable difficulty separation.
- The relative robustness of different modalities (RGB,

TIR, RGB+TIR) is highly sensitive to occlusion, making these subsets suitable for studying how multi-modal fusion mitigates missing visual evidence.

- Method rankings under PO and HO are largely consistent across RefFLIR, RefM³FD, and RefMFAD, suggesting that the occlusion annotations provide reliable, dataset-agnostic evaluation signals.

A.8. Summary

Across all extended evaluations on scene semantics, weather, illumination, object size, and occlusion, we obtain the following consistent observations:

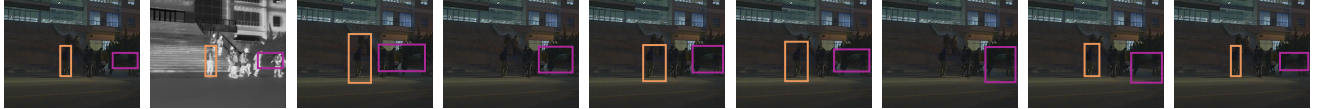
- **Environmental difficulty spectra.** The five types of annotations together form meaningful and stable difficulty spectra. Challenging conditions such as rural and tunnel scenes, foggy and rainy weather, weak or very weak illumination, small objects, and heavy occlusion all lead to significant performance drops for most methods, whereas structurally simple or well-lit settings are comparatively easier. This confirms that the multi-level factors in RGBT-Ground effectively stress different aspects of visual grounding robustness.
- **Multi-modal models vs. single-modality models.** Multimodal RGB-TIR models consistently outperform RGB-only and TIR-only counterparts across almost all environmental and contextual subsets. RGB-only methods are strong in favorable conditions but degrade sharply when visibility is compromised; TIR-only methods are more stable in low-light or adverse weather but lack fine-grained semantics in easy regimes. RGB-TIR fusion achieves the best trade-off, demonstrating that thermal information is not only useful in extreme cases (e.g., very low light), but also provides complementary cues in normal settings.
- **Role of complementary modalities.** The complementary nature of RGB and TIR is particularly crucial under **low-light**, **foggy**, **heavy-occlusion**, and **small-object** conditions, where appearance cues from a single modality become unreliable or ambiguous. In these challenging subsets, RGB-TIR fusion not only improves absolute performance but also reduces the performance gap between easy and hard cases, making RGBT-Ground a suitable testbed for studying when and how additional sensing modalities should be exploited.
- **Robustness of RGBT-VGNet.** The proposed **RGBT-VGNet** consistently ranks among the top performers across more than 25 fine-grained subsets (13 scene types, 4 weather conditions, 4 illumination levels, 2 occlusion levels, and 2 object sizes) on all three RGBT-Ground sub-datasets. Its gains are especially pronounced in the most challenging regimes, such as rural and tunnel scenes, foggy and rainy weather, weak or very weak illumination, small objects, and heavy occlusion. These results indicate



1. Person riding a bike, partially obscured by fog. 2. Bike with visible rear light positioned near road edge, partially obscured by fog. 3. A black sedan parked on the left of the street under a streetlight.



1. A small silver truck appears ahead near center-left lane in a tunnel. 2. A silver sedan drives ahead through the tunnel's illuminated corridor.



1. Person in dark clothing stands near a library stair, facing away. 2. A dark SUV is parked far from the crowd near the library, facing forward.



1. Person in dark clothing stands near a white car, probably holding a phone. 2. A white SUV with a sleek design is parked on a cobblestone street near a residential area, facing forward.



1. A dark-colored sedan parked in a lot near other vehicles. 2. A person in blue shirt and dark pants walks near a residential area.



1. A long bus travels down the wet road, its lights reflecting on the pavement. 2. A silver minivan is parked on the wet roadside under a tree. 3. A person in a red top and dark pants walks with arms raised in the rainy day.



1. A red double-decker bus with advertisements occupies part of the lane near traffic lights under skies. 2. A small white sedan drives along the road, positioned centrally among other vehicles under foggy skies. 3. A small figure wearing yellow clothing stands near the right edge of the road.

Figure 6. Additional qualitative comparison of multi-modal RGBT visual grounding results on RGBT-Ground across diverse real-world scenarios. Bounding box colors match the description below. Each column shows a different visual grounding method, stressing differences across methods under diverse scenes, illumination, weather, object size, and occlusion.

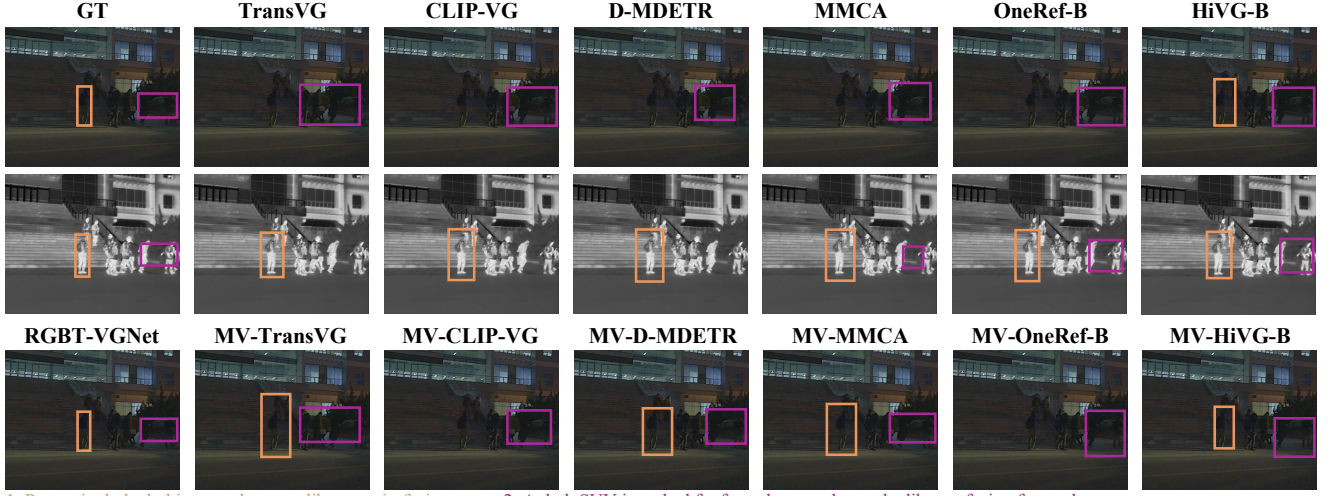
that the combination of AMA and LAVS is effective not only for improving average accuracy, but also for stabilizing performance under severe domain shifts, where either RGB or TIR alone becomes unreliable. In this sense, RGBT-VGNet provides a strong and reproducible baseline for future work on RGB-TIR visual grounding.

- **Benchmark value of RGBT-Ground.** The relative ranking of competing methods remains largely consistent across different subsets and across the three sub-datasets (RefFLIR, RefM³FD, RefMFAD), despite their differences in acquisition conditions. This suggests that RGBT-Ground provides stable, dataset-agnostic measurements of model capability, rather than being dominated by idiosyncrasies of a single domain. Moreover, the multi-

level annotations along scene, weather, illumination, size, and occlusion dimensions enable systematic analysis of failure modes, modality contributions, and design choices (e.g., single-modality vs. multi-modal fusion, zero-shot vs. fine-tuned training). Taken together, these properties make RGBT-Ground a comprehensive and reliable benchmark for fairly comparing future RGB-TIR visual grounding approaches under diverse and controllable real-world conditions.

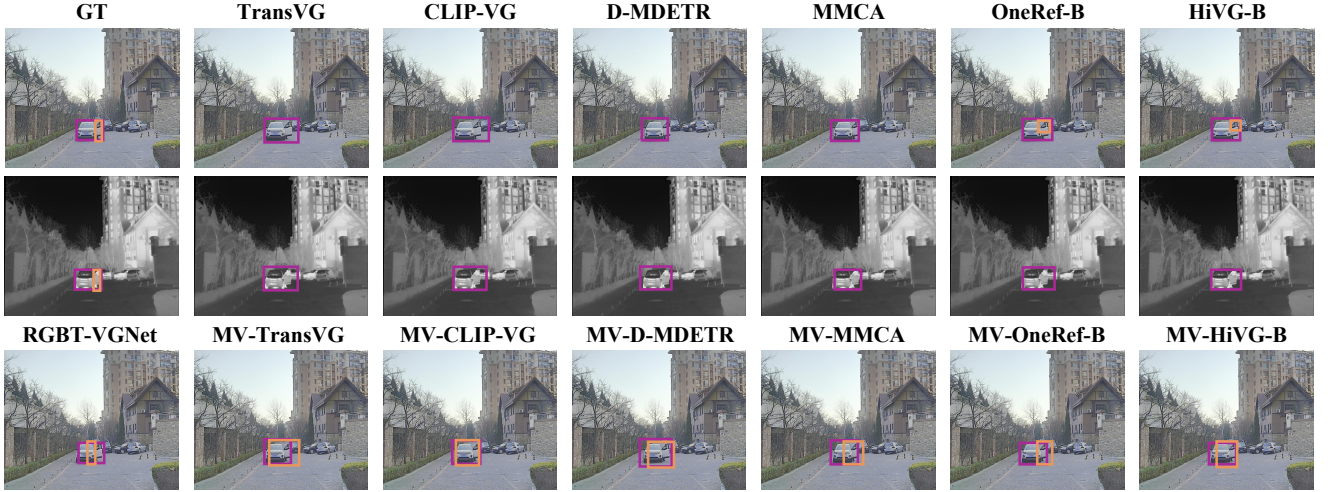
B. More Qualitative Comparison Experiments

As shown in Figure 6, we present additional qualitative visualization results obtained from multi-modal RGBT



1. Person in dark clothing stands near a library stair, facing away. 2. A dark SUV is parked far from the crowd near the library, facing forward.

Figure 7. Qualitative comparison of RGB-only, TIR-only and RGB-TIR grounding results (Figure 6 row 3) on RGBT-Ground across diverse real-world scenarios. Bounding box colors match the description below. Each column shows a different visual grounding method, stressing differences across methods under diverse scenes, illumination, weather, object size, and occlusion.



1. Person in dark clothing stands near a white car, probably holding a phone. 2. A white SUV with a sleek design is parked on a cobblestone street near a residential area, facing forward.

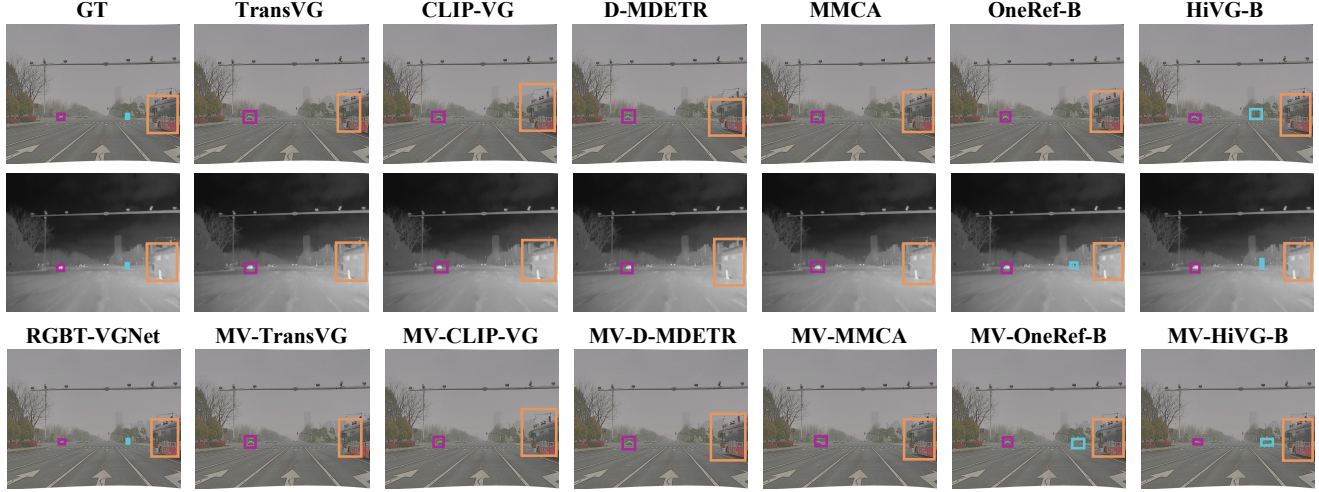
Figure 8. Qualitative comparison of RGB-only, TIR-only and RGB-TIR grounding results (Figure 6 row 4) on RGBT-Ground across diverse real-world scenarios. Bounding box colors match the description below. Each column shows a different visual grounding method, stressing differences across methods under diverse scenes, illumination, weather, object size, and occlusion.

grounding methods of RGBT-VG framework across a wide range of scenarios in the RGBT-Ground benchmark. These examples illustrate how multi-modal RGBT visual grounding models behave under diverse real-world environmental variations and highlight the types of challenges represented in the benchmark.

Nighttime and Extremely Low-Light Conditions. As shown in Figure 6 (row 1 and 3), nighttime scenes exhibit severe degradation in RGB appearance due to low illumination, noise, and missing texture. Thermal imagery, how-

ever, retains clear contours. The multi-modal predictions show that RGBT models maintain reliable localization even when visible-light cues collapse. As a representative RGBT method, RGBT-VGNet shows particularly stable behavior in these examples, where its adaptive fusion helps extract useful thermal patterns without overrelying on degraded RGB inputs.

Tunnel Scenarios with Illumination Changes. As shown in Figure 6 (row 2), tunnel scenes involve a clear different from artificial lighting to natural daylight inside the tun-



1. A red double-decker bus with advertisements occupies part of the lane near traffic lights under skies. 2. A small white sedan drives along the road, positioned centrally among other vehicles under foggy skies. 3. A small figure wearing yellow clothing stands near the right edge of the road.

Figure 9. Qualitative comparison of RGB-only, TIR-only and RGB-TIR grounding results (Figure 6 row 7) on RGBT-Ground across diverse real-world scenarios. Bounding box colors match the description below. Each column shows a different visual grounding method, stressing differences across methods under diverse scenes, illumination, weather, object size, and occlusion.

nel. This change causes large appearance variations in the RGB images, including shifts in color temperature, contrast, and shading, which makes it harder to maintain consistent visual features along the lane. In contrast, the thermal modality remains relatively stable across the entire sequence. The multi-modal predictions indicate that RGBT-VGNet can emphasize these stable thermal cues while selectively exploiting RGB textures when the illumination becomes more reliable, illustrating the benefit of asymmetric modality adaptation in such dynamically lit environments.

Closed-Road Scenarios. As shown in Figure 6 (row 3, 4, and 5) and Figure 7, these scenes correspond to semi-enclosed or restricted roads such as campus driveways, residential side streets, and internal access lanes. They typically exhibit complex man-made structures, varied background layouts (buildings, fences, trees, and parked vehicles), and strong perspective distortions along the road. In such environments, multi-modal predictions are able to follow spatial and relational phrases in the language expressions (e.g., “near the stairs” or “ahead in the lane”), even when multiple plausible candidates exist along the same trajectory. We observe that RGBT-VGNet often produces more precise localization when the description relies on subtle spatial relations, suggesting that its language-aware design helps identify contextually relevant regions and disambiguate targets in these closed-road scenarios.

Occlusion-Heavy Objects. As shown in Figure 6 (row 4) and Figure 8, dense objects and frequent partial occlusions. The multi-modal results show that RGBT inputs help preserve the visibility of people or vehicles even when RGB textures are partially blocked. In such cases, RGBT-VGNet

tends to maintain stronger spatial consistency, likely due to the synergistic use of thermal and language guidance.

Foggy, Rainy and Diverse Weather. As shown in Figure 6 (row 1, 6, and 7). Fog and mist cause strong scattering in RGB images, washing out objects boundaries and reducing contrast. The visualizations demonstrate that multi-modal inputs help restore spatial coherence by leveraging thermal responses that remain mostly unaffected. We also observe that RGBT-VGNet tends to generate more compact and consistent bounding boxes under foggy conditions, benefiting from its language-aware fusion that guides cross-modal alignment.

C. Ablation on RGBT-VGNet Components

As shown in Table 6, we conduct a series of controlled ablation experiments to evaluate the contribution of each component in the proposed RGBT-VGNet baseline. By selectively removing or disabling key modules, we aim to understand the functional role of each design choice and analyze how they collaboratively benefit RGBT visual grounding.

Effectiveness of the AMA module. Introducing the Asymmetric Modality Adaptation (AMA) module brings a clear performance improvement across all three datasets (Ref-FLIR, RefM³FD, RefMFAD) and across all difficulty levels (testA/B/C). Without AMA, the model must fuse RGB and TIR features in their raw feature spaces, where the strong domain gap between visible and thermal imagery leads to unstable feature alignment. The results in the first row of Table 6 show that, under this setting, TIR information is not effectively exploited, and in several cases, even degrades performance due to noisy or inconsistent thermal patterns.

Table 6. **Ablation of AMA and LAVS in RGBT-VGNet.** AMA substantially improves performance over the baseline by mitigating the RGB-TIR domain gap, and adding LAVS further boosts results, particularly on low-light (testB) and small-object (testC) splits across RefFLIR, RefM³FD, and RefMFAD.

AMA	LAVS	RefFLIR					RefM ³ FD					RefMFAD				
		val	test	testA	testB	testC	val	test	testA	testB	testC	val	test	testA	testB	testC
✓		55.42	46.19	67.42	41.56	22.81	54.16	57.57	78.89	65.63	34.46	53.50	54.63	81.77	51.91	36.62
✓	✓	74.01	71.17	90.57	66.25	49.69	70.83	72.53	93.99	80.16	50.43	68.07	65.27	90.63	62.19	47.96
		73.68	72.65	91.31	67.19	52.23	73.21	74.34	94.72	81.93	53.63	67.83	66.62	91.16	64.07	49.76

With AMA enabled (second row), the model learns to adapt the two modalities into a more compatible feature space, allowing the fused representation to benefit from complementary cues in low-light, foggy, and occlusion-heavy scenes.

Effectiveness of the LAVS module. Adding the Language-Aware Visual Synergy (LAVS) module further improves performance on nearly all subsets, especially on low-light (testB) and small-object (testC) partitions. LAVS enhances the model’s ability to select modality-relevant regions based on language guidance, enabling more accurate grounding in scenes where RGB or TIR alone may be insufficient. The improvements suggest that semantic alignment between text and cross-modal visual features is a crucial factor for achieving robust localization.

Why no “LAVS-only” ablation? We intentionally do not include a configuration that keeps LAVS while removing AMA. This is because, without AMA, the CLIP-based backbone faces a substantial domain gap when processing TIR images. Raw thermal features are poorly aligned with RGB semantics, and feeding such unadapted TIR features directly into a fusion module leads to severe feature contamination. Under this condition, enabling LAVS cannot provide meaningful language-guided fusion; instead, it would amplify noise from the misaligned TIR modality and destabilize grounding performance. In other words, AMA is a prerequisite for extracting informative TIR representations. Without reducing the cross-modal domain discrepancy, LAVS alone cannot be meaningfully evaluated, as the resulting model behaves unpredictably, even worse than RGB-only.

Summary. Overall, the ablation results demonstrate that AMA plays a foundational role by enabling effective cross-modal feature adaptation, while LAVS provides an additional layer of language-guided refinement. Together, they form a complementary design that supports the robustness of RGBT-VGNet across complex real-world scenarios

D. Complete Data Annotation Process

D.1. Scene and Weather Annotation Prompt

To comprehensively characterize the global context of each image, we designed a scene-level annotation prompt that

captures four key environmental attributes. The specific template of this prompt is as follows:

Comprehensively analyze the global scene context of the provided image and return exactly four numerical codes representing the following environmental attributes:

- (1) Scene:
0-(Urban),
1-(Suburban),
2-(Rural),
3-(Highway),
4-(Residential),
5-(Industrial),
6-(Parking),
7-(Intersection),
8-(Tunnel),
9-(Bridge),
10-(Campus),
11-(Market),
12-(Waterfront)
- (2) Weather:
0-(Foggy),
1-(Rainy),
2-(Sunny),
3-(Cloudy)

Return only four numbers without additional text (space-separated).

This holistic analysis provides essential contextual information for understanding the operational environment in multi-sensor visual grounding tasks.

D.2. Lighting Annotation Prompt

The lighting annotation prompt aims to capture the global illumination level of each scene. By classifying images into four brightness levels, this prompt helps quantify how illumination affects RGB, TIR, and RGB-TIR providing essential metadata for analyzing modality robustness under varying lighting environments

You are an expert at analyzing lighting conditions in images. I will provide an image, and your task is to classify the overall lighting intensity of the image into one of the following categories:

0. Very Weak Light: The image is mostly dark, but some features can be faintly seen.
1. Weak Light: The image has low visibility, typical for dawn or dusk.

2. Normal Light: The image has normal daylight brightness.
3. Strong Light: The image is brightly lit, typically from midday sunlight.

Please return only one number corresponding to the lighting condition: 0 (very_weak_light), 1 (weak_light), 2 (normal_light), or 3 (strong_light).

Now, please begin generating the number

D.3. Object-Level Annotation Prompts and Rules

Object-level annotations provide a fine-grained characterization of individual instances within the scene. This level is further decomposed into three components to ensure comprehensive object understanding.

Object referring expressions. This component generates dense, structured textual descriptions that encapsulate multiple aspects of each object instance, including visual appearance, spatial relationships, and functional attributes. The specific template of this prompt is as follows:

```
I will provide an image and the bounding box
coordinates (bbox) of a {category_name}. Your
task is to describe the object within the
bounding box in one concise sentence,
focusing on its appearance and key features.

1. Object Details: Please describe the object in
detail, including but not limited to its
appearance, color, shape, texture, size, and
posture.

2. Contextual Relationship: If there is any
relationship between the objects within the
image or between the object and the
background (e.g., relative positioning,
interaction), please reflect this in your
description.

3. Distinguishing Similar Objects: If there are
multiple similar objects in the image,
differentiate them by comparing their details
such as color intensity, position, state,
etc.

4. Concise and Clear Language: Provide a single,
concise sentence that captures the key
features without breaking down into different
aspects. The description should be rich in
information yet simple for later data
processing.
```

Please generate only one few words of description
for the {category_name} with the following
bounding box coordinates:[{bbox}]

Now, please begin generating the description:

Occlusion annotation The occlusion analysis component assesses the visibility level of each object instance. The specific template of this prompt is as follows:

```
Analyze the occlusion level of the specified
object and return exactly one integer value:
0 - No occlusion: The object is fully visible
1 - Partial occlusion: Some parts are obscured
but key features remain visible
2 - Heavy occlusion: More than 50% of the object
is obscured
```

Target object bounding box: [x1, y1, x2, y2]

Return only 0, 1, or 2 without additional text.

Object Size Classification The size classification employs a computational approach based on bounding box area percentage, categorizing objects into two distinct classes. The classification algorithm is implemented as follows:

Table 7. Object Size Classification Criteria

Category	Area Percentage
Small	<1%
Normal	≥1%

```
def classify_object_size(bbox, img_width,
img_height):
    x, y, w, h = bbox # bbox format: [x, y,
    width, height]
    bbox_area = w * h
    image_area = img_width * img_height
    size_ratio = bbox_area / image_area

    return "small" if size_ratio < 0.01 else "
normal"
```

This hierarchical annotation framework enables comprehensive multi-modal understanding while maintaining computational efficiency. The scene-level annotations provide global context, while the object-level components (occlusion analysis, comprehensive description, and size classification) offer detailed instance characterization essential for robust visual grounding performance.

E. Potential Applications of the RGBT-Ground

Beyond the primary task of referring expression grounding, the RGBT-Ground benchmark provides rich multi-modal information that can support a wide range of vision-language applications. In this section, we outline several potential extensions and discuss how the dataset structure naturally lends itself to broader research tasks.

E.1. Referring Expression Segmentation (RES)

The bounding-box annotations in RGBT-Ground, paired with natural language referring expressions, naturally support *weakly supervised* Referring Expression Segmentation (RES). Given the RGB-TIR paired images, one can generate pseudo segmentation masks using off-the-shelf tools such as SAM, Mask2Former, or GrabCut, and subsequently use these masks as training signals for RES models.

The multi-modal RGB-TIR setting is particularly attractive for RES under low-light, foggy, or heavily occluded conditions, where RGB-only segmentation models struggle to delineate object boundaries, while TIR images still provide stable, high-contrast contours. This suggests that RGBT-Ground could be extended into a multi-modal RES benchmark for evaluating segmentation performance in adverse environments.

E.2. Visual Question Answering (VQA)

The natural language expressions in RGBT-Ground contain relational cues, positional descriptions, and object attributes, which can be converted into VQA-style question–answer pairs. Examples include:

- **Binary VQA:** “Is the person behind the car present?”
- **Counting:** “How many vehicles are mentioned?”
- **Localization VQA:** “Where is the referenced pedestrian located?”

RGB–TIR pairs provide strong visual grounding signals for such reasoning-oriented questions, especially under low-light or high-occlusion scenarios where RGB-only VQA systems typically fail. This makes RGBT-Ground a promising testbed for investigating multi-modal reasoning and robust VQA in safety-critical settings.

E.3. Cross-Modal Retrieval

RGBT-Ground also supports various retrieval tasks:

- **Text-to-image retrieval:** using expressions as retrieval queries;
- **Image-to-text retrieval:** using object-level bounding boxes as visual queries;
- **RGB–TIR to language retrieval:** jointly exploiting both modalities.

These tasks benefit from the fine-grained textual descriptions and multi-level environmental annotations (scene, weather, illumination, occlusion, size) provided by the benchmark.

Summary. Overall, RGBT-Ground is not limited to grounding; it provides a unified dataset for studying multi-modal perception, cross-modal reasoning, and language-guided understanding under diverse and challenging real-world conditions, and can serve as a foundation for a broad family of downstream vision–language tasks.

Table 8. **Scene-level Acc@0.5 across 13 scene types** (UB, IT, RS, SU, HW, CP, BG, PL, RR, TN, MK, WF, ID) on the RefFLIR sub-dataset of RGBT-Ground. All methods, backbones, and modalities are included, following the style of Table 4 and Table 5 in the manuscript. Noted that the ‘/’ symbol indicates that there is no data of the corresponding type in the current sub-dataset.

Method	Visual / Language Backbone	Modality	RefFLIR (Scene Types)												
			UB	SU	RR	HW	RS	ID	PL	IT	TN	BG	CP	MK	WF
a. Pretrained model zero-shot transfer setting:															
CLIP-VG [33]	CLIP-B / CLIP-B	RGB	6.56	5.37	/	100.00	6.41	/	10.56	7.02	20.00	4.41	/	7.89	14.33
HiVG-B [35]	CLIP-B / CLIP-B	RGB	33.12	36.36	/	0.00	37.18	/	47.22	34.13	30.00	16.18	/	32.24	32.75
HiVG-L [35]	CLIP-L / CLIP-L	RGB	37.50	40.50	/	100.00	50.00	/	58.89	40.59	40.00	44.12	/	38.82	56.14
OneRef-B [36]	BEIT3-B / BEIT3-B	RGB	36.25	43.39	/	100.00	51.28	/	56.11	39.33	60.00	19.12	/	36.18	48.25
OneRef-L [36]	BEIT3-L / BEIT3-L	RGB	37.81	52.48	/	100.00	62.82	/	63.33	46.91	50.00	42.65	/	40.79	59.36
CLIP-VG [33]	CLIP-B / CLIP-B	TIR	7.50	5.79	/	0.00	3.85	/	6.11	8.43	0.00	2.94	/	11.84	11.40
HiVG-B [35]	CLIP-B / CLIP-B	TIR	16.88	13.22	/	0.00	11.54	/	12.22	13.48	10.00	1.47	/	12.50	10.53
HiVG-L [35]	CLIP-L / CLIP-L	TIR	26.25	21.90	/	100.00	30.77	/	32.22	21.63	10.00	7.35	/	19.08	32.46
OneRef-B [36]	BEIT3-B / BEIT3-B	TIR	26.25	27.69	/	100.00	32.05	/	33.33	26.97	20.00	2.94	/	20.39	28.95
OneRef-L [36]	BEIT3-L / BEIT3-L	TIR	27.19	28.93	/	100.00	33.33	/	36.11	27.25	20.00	8.82	/	14.47	28.65
b. Single source dataset training setting:															
TransVG [6]	RN50+DETR / BERT-B	RGB	42.19	59.50	/	100.00	62.82	/	33.33	40.03	60.00	29.41	/	40.79	38.60
CLIP-VG [33]	CLIP-B / CLIP-B	RGB	23.12	30.17	/	0.00	37.18	/	22.78	22.47	40.00	20.59	/	23.03	26.02
D-MDETR [29]	CLIP-B / CLIP-B	RGB	44.69	64.88	/	100.00	64.94	/	44.44	48.60	70.00	48.53	/	46.05	45.91
D-MDETR [29]	RN50+DETR / BERT-B	RGB	41.25	57.85	/	100.00	64.94	/	43.33	44.24	70.00	25.00	/	36.84	41.23
MMCA [41]	RN50+DETR / BERT-B	RGB	42.50	57.44	/	100.00	68.83	/	43.89	44.94	70.00	36.76	/	43.42	47.08
HiVG-B [35]	CLIP-B / CLIP-B	RGB	54.06	75.62	/	100.00	79.49	/	72.78	63.62	70.00	75.00	/	58.55	69.30
HiVG-L [35]	CLIP-L / CLIP-L	RGB	62.81	76.86	/	100.00	88.46	/	77.78	67.13	80.00	73.53	/	62.50	73.68
OneRef-B [36]	BEIT3-B / BEIT3-B	RGB	54.69	71.90	/	100.00	71.79	/	71.67	59.55	70.00	66.18	/	55.92	62.57
OneRef-L [36]	BEIT3-L / BEIT3-L	RGB	53.75	73.55	/	100.00	76.92	/	77.22	63.34	70.00	75.00	/	55.92	65.79
TransVG [6]	RN50+DETR / BERT-B	TIR	41.25	56.20	/	100.00	65.38	/	34.44	41.57	60.00	38.24	/	38.16	39.77
CLIP-VG [33]	CLIP-B / CLIP-B	TIR	37.81	43.39	/	100.00	50.00	/	42.78	36.52	50.00	16.18	/	30.26	36.26
D-MDETR [29]	CLIP-B / CLIP-B	TIR	48.75	59.50	/	100.00	59.74	/	41.11	45.08	80.00	29.41	/	45.39	40.06
D-MDETR [29]	RN50+DETR / BERT-B	TIR	48.12	54.13	/	100.00	59.74	/	42.22	44.38	60.00	16.18	/	33.55	34.80
MMCA [41]	RN50+DETR / BERT-B	TIR	43.75	56.20	/	100.00	59.74	/	36.11	40.45	60.00	22.06	/	36.84	36.26
HiVG-B [35]	CLIP-B / CLIP-B	TIR	62.19	64.88	/	100.00	73.08	/	54.44	59.83	70.00	42.65	/	50.66	51.17
HiVG-L [35]	CLIP-L / CLIP-L	TIR	62.81	76.86	/	100.00	88.46	/	77.78	67.13	80.00	73.53	/	62.50	73.68
OneRef-B [36]	BEIT3-B / BEIT3-B	TIR	63.44	68.60	/	100.00	73.08	/	60.00	60.53	80.00	41.18	/	53.95	55.26
OneRef-L [36]	BEIT3-L / BEIT3-L	TIR	62.50	68.18	/	100.00	76.92	/	60.56	62.08	70.00	44.12	/	59.87	56.73
MV-TransVG	RN50+DETR / BERT-B	RGB+TIR	45.31	58.68	/	100.00	69.23	/	42.78	45.65	60.00	35.29	/	37.50	42.98
MV-CLIP-VG	CLIP-B / CLIP-B	RGB+TIR	38.44	47.93	/	100.00	53.85	/	42.78	38.20	60.00	27.94	/	40.79	41.81
MV-D-MDETR	CLIP-B / CLIP-B	RGB+TIR	48.44	58.68	/	100.00	66.23	/	40.00	46.91	70.00	35.29	/	44.74	44.74
MV-D-MDETR	RN50+DETR / BERT-B	RGB+TIR	48.75	56.20	/	100.00	67.53	/	42.78	48.74	60.00	33.82	/	42.76	44.15
MV-MMCA	RN50+DETR / BERT-B	RGB+TIR	45.00	61.16	/	100.00	66.23	/	48.33	47.89	70.00	44.12	/	46.05	45.91
MV-HiVG-B	CLIP-B / CLIP-B	RGB+TIR	66.88	73.14	/	100.00	76.92	/	73.89	66.85	80.00	64.71	/	62.50	65.20
MV-HiVG-L	CLIP-L / CLIP-L	RGB+TIR	72.19	79.75	/	100.00	<u>83.33</u>	/	<u>73.89</u>	74.02	90.00	<u>73.53</u>	/	64.47	76.90
MV-OneRef-B	BEIT3-B / BEIT3-B	RGB+TIR	58.75	67.36	/	100.00	78.21	/	71.67	60.81	70.00	52.94	/	55.92	60.82
MV-OneRef-L	BEIT3-L / BEIT3-L	RGB+TIR	55.62	72.31	/	100.00	74.36	/	65.00	59.83	70.00	51.47	/	57.89	60.23
RGBT-VGNet (Ours)	CLIP-B / CLIP-B	RGB+TIR	71.56	<u>78.10</u>	/	100.00	87.18	/	78.89	<u>69.52</u>	80.00	76.47	/	65.79	<u>75.15</u>

Table 9. **Scene-level Acc@0.5 across 13 scene types** (UB, IT, RS, SU, HW, CP, BG, PL, RR, TN, MK, WF, ID) on the RefM3FD sub-dataset of RGBT-Ground. All methods, backbones, and modalities are included, following the style of Table 4 and Table 5 in the manuscript.

Method	Visual / Language Backbone	Modality	RefM3FD (Scene Types)												
			UB	SU	RR	HW	RS	ID	PL	IT	TN	BG	CP	MK	WF
a. Pretrained model zero-shot transfer setting:															
CLIP-VG [33]	CLIP-B / CLIP-B	RGB	10.22	7.78	3.45	23.81	8.78	0.00	8.43	9.43	5.68	4.17	5.49	2.34	2.74
HiVG-B [35]	CLIP-B / CLIP-B	RGB	33.63	19.16	41.95	34.52	46.62	10.00	37.95	37.30	23.86	9.38	19.08	38.28	23.29
HiVG-L [35]	CLIP-L / CLIP-L	RGB	31.43	17.66	27.01	29.76	33.78	60.00	36.14	40.57	17.05	25.00	30.35	22.66	15.75
OneRef-B [36]	BEIT3-B / BEIT3-B	RGB	42.20	19.76	33.33	38.10	55.41	60.00	60.84	48.36	34.09	21.88	36.71	42.19	24.66
OneRef-L [36]	BEIT3-L / BEIT3-L	RGB	48.90	28.74	50.57	42.86	67.57	60.00	59.64	54.92	22.73	23.96	50.58	46.88	30.82
CLIP-VG [33]	CLIP-B / CLIP-B	TIR	6.87	4.79	17.82	13.10	4.73	0.00	7.23	9.43	0.00	1.04	4.05	1.56	4.79
HiVG-B [35]	CLIP-B / CLIP-B	TIR	13.41	5.39	8.05	10.71	12.84	0.00	15.66	20.08	6.82	7.29	5.49	12.50	5.48
HiVG-L [35]	CLIP-L / CLIP-L	TIR	54.56	30.84	56.32	59.52	72.30	60.00	64.46	52.46	40.91	37.50	66.18	51.56	36.99
OneRef-B [36]	BEIT3-B / BEIT3-B	TIR	25.49	12.87	13.79	27.38	26.35	60.00	30.12	34.02	20.45	10.42	17.92	22.66	8.90
OneRef-L [36]	BEIT3-L / BEIT3-L	TIR	24.07	15.27	17.82	23.81	33.78	60.00	31.93	38.52	10.23	7.29	26.01	20.31	14.38
b. Single source dataset training setting:															
TransVG [6]	RN50+DETR / BERT-B	RGB	41.54	21.86	67.82	47.62	52.03	60.00	50.00	40.16	39.77	14.58	39.02	35.94	25.34
CLIP-VG [33]	CLIP-B / CLIP-B	RGB	33.46	18.86	32.76	34.52	38.51	60.00	49.40	36.07	23.86	10.42	32.08	21.88	12.33
D-MDETR [29]	CLIP-B / CLIP-B	RGB	50.74	37.72	73.41	60.71	64.63	66.67	65.06	40.98	48.28	22.92	58.84	35.43	32.41
D-MDETR [29]	RN50+DETR / BERT-B	RGB	-	-	-	-	-	-	-	-	-	-	-	-	-
MMCA [41]	RN50+DETR / BERT-B	RGB	-	-	-	-	-	-	-	-	-	-	-	-	-
HiVG-B [35]	CLIP-B / CLIP-B	RGB	66.54	49.70	79.89	71.43	75.00	60.00	81.33	65.57	53.41	50.00	73.41	60.94	44.52
HiVG-L [35]	CLIP-L / CLIP-L	RGB	67.97	48.50	80.46	72.62	80.41	60.00	80.72	63.93	53.41	58.33	73.41	60.94	43.15
OneRef-B [36]	BEIT3-B / BEIT3-B	RGB	68.90	50.30	82.18	72.62	82.43	60.00	83.13	61.07	54.55	58.33	73.12	64.06	50.00
OneRef-L [36]	BEIT3-L / BEIT3-L	RGB	66.59	43.11	72.99	69.05	75.00	60.00	84.34	62.30	53.41	52.08	68.50	61.72	47.95
TransVG [6]	RN50+DETR / BERT-B	TIR	48.46	32.04	75.86	57.14	60.81	60.00	63.25	45.90	43.18	15.62	49.71	42.97	25.34
CLIP-VG [33]	CLIP-B / CLIP-B	TIR	29.12	12.57	35.06	27.38	31.08	60.00	47.59	29.92	18.18	7.29	28.32	21.09	13.70
D-MDETR [29]	CLIP-B / CLIP-B	TIR	51.18	37.13	79.77	60.71	61.90	100.00	65.06	38.52	52.87	19.79	56.81	39.37	30.34
D-MDETR [29]	RN50+DETR / BERT-B	TIR	-	-	-	-	-	-	-	-	-	-	-	-	-
MMCA [41]	RN50+DETR / BERT-B	TIR	-	-	-	-	-	-	-	-	-	-	-	-	-
HiVG-B [35]	CLIP-B / CLIP-B	TIR	64.12	48.20	81.61	67.86	72.97	80.00	83.73	61.07	59.09	42.71	70.23	56.25	35.62
HiVG-L [35]	CLIP-L / CLIP-L	TIR	63.74	50.60	85.63	71.43	75.68	80.00	75.30	65.16	54.55	46.88	74.57	58.59	39.04
OneRef-B [36]	BEIT3-B / BEIT3-B	TIR	66.59	49.10	82.76	71.43	70.27	80.00	86.14	61.48	57.95	50.00	72.25	60.94	35.62
OneRef-L [36]	BEIT3-L / BEIT3-L	TIR	68.96	52.69	85.63	73.81	81.08	100.00	85.54	62.70	59.09	56.25	74.57	66.41	47.95
MV-TransVG	RN50+DETR / BERT-B	RGB+TIR	48.41	33.53	80.46	57.14	58.78	60.00	61.45	47.54	43.18	18.75	52.02	39.06	27.40
MV-CLIP-VG	CLIP-B / CLIP-B	RGB+TIR	40.82	20.06	45.98	45.24	50.00	60.00	59.64	45.49	34.09	15.62	40.46	28.91	21.23
MV-D-MDETR	CLIP-B / CLIP-B	RGB+TIR	47.72	32.34	72.23	55.95	57.82	77.78	59.64	38.93	48.28	19.79	51.88	35.43	25.52
MV-D-MDETR	RN50+DETR / BERT-B	RGB+TIR	45.08	30.84	79.77	57.14	61.90	66.67	56.02	37.30	44.83	16.67	54.49	38.58	27.59
MV-MMCA	RN50+DETR / BERT-B	RGB+TIR	49.53	31.44	69.36	51.19	61.22	66.67	63.86	45.90	37.93	15.62	52.46	43.31	26.90
MV-HiVG-B	CLIP-B / CLIP-B	RGB+TIR	71.98	53.89	87.93	<u>77.38</u>	79.05	100.00	87.35	66.39	56.82	54.17	<u>78.61</u>	64.84	49.32
MV-HiVG-L	CLIP-L / CLIP-L	RGB+TIR	<u>73.74</u>	53.59	89.08	76.19	<u>81.76</u>	70.00	<u>89.16</u>	73.36	<u>60.23</u>	<u>60.42</u>	<u>78.61</u>	64.06	43.84
MV-OneRef-B	BEIT3-B / BEIT3-B	RGB+TIR	65.82	46.71	82.18	73.81	77.70	80.00	81.33	59.02	52.27	53.12	69.08	60.94	43.15
MV-OneRef-L	BEIT3-L / BEIT3-L	RGB+TIR	70.22	53.89	<u>90.23</u>	73.81	80.41	100.00	87.35	62.70	55.68	53.12	77.17	<u>69.53</u>	<u>54.11</u>
RGBT-VGNet (Ours)	CLIP-B / CLIP-B	RGB+TIR	74.84	57.49	91.95	78.57	83.78	90.00	92.17	68.03	61.36	63.54	81.50	73.44	58.90

Table 10. **Scene-level Acc@0.5 across 13 scene types** (UB, IT, RS, SU, HW, CP, BG, PL, RR, TN, MK, WF, ID) on the RefMFAD sub-dataset of RGBT-Ground. All methods, backbones, and modalities are included, following the style of Table 4 and 5 in the manuscript.

Method	Visual / Language Backbone	Modality	RefMFAD (Scene Types)												
			UB	SU	RR	HW	RS	ID	PL	IT	TN	BG	CP	MK	WF
a. Pretrained model zero-shot transfer setting:															
CLIP-VG [33]	CLIP-B / CLIP-B	RGB	7.94	9.53	7.69	7.41	4.92	16.67	4.35	8.16	4.12	6.93	3.81	0.00	0.00
HiVG-B [35]	CLIP-B / CLIP-B	RGB	7.21	6.51	0.00	9.09	9.02	11.11	15.22	5.93	9.28	8.91	8.57	0.00	0.00
HiVG-L [35]	CLIP-L / CLIP-L	RGB	42.06	34.88	32.69	42.76	42.62	27.78	63.04	35.16	32.99	48.02	40.95	50.00	66.67
OneRef-B [36]	BEIT3-B / BEIT3-B	RGB	31.33	26.98	23.08	27.95	31.97	22.22	54.35	28.19	25.26	29.70	34.76	33.33	66.67
OneRef-L [36]	BEIT3-L / BEIT3-L	RGB	38.42	37.21	23.08	38.05	33.61	27.78	45.65	35.16	28.35	36.63	38.10	33.33	83.33
CLIP-VG [33]	CLIP-B / CLIP-B	TIR	6.87	4.79	17.82	13.10	4.73	0.00	7.23	9.43	0.00	1.04	4.05	1.56	4.79
HiVG-B [35]	CLIP-B / CLIP-B	TIR	20.61	16.05	13.46	21.55	18.03	16.67	22.83	18.55	22.68	19.80	19.05	33.33	50.00
HiVG-L [35]	CLIP-L / CLIP-L	TIR	23.33	20.47	17.31	20.88	22.95	11.11	42.39	21.22	29.90	26.24	24.76	33.33	0.00
OneRef-B [36]	BEIT3-B / BEIT3-B	TIR	16.67	12.33	13.46	13.30	18.03	16.67	33.70	12.76	17.53	15.84	19.52	0.00	66.67
OneRef-L [36]	BEIT3-L / BEIT3-L	TIR	18.30	15.35	9.62	18.35	17.21	16.67	35.87	15.73	15.46	18.32	21.90	0.00	50.00
b. Single source dataset training setting:															
TransVG [6]	RN50+DETR / BERT-B	RGB	47.21	49.30	46.15	56.73	36.89	50.00	61.96	41.99	64.95	53.96	41.90	33.33	83.33
CLIP-VG [33]	CLIP-B / CLIP-B	RGB	38.97	34.88	32.69	39.39	25.41	22.22	50.00	34.27	47.94	42.08	26.19	33.33	66.67
D-MDETR [29]	CLIP-B / CLIP-B	RGB	57.91	64.88	73.08	65.60	49.18	44.44	68.45	52.30	75.77	57.43	53.11	60.00	60.00
D-MDETR [29]	RN50+DETR / BERT-B	RGB	49.30	52.79	50.00	60.37	44.26	38.89	57.61	44.13	67.53	56.44	41.63	60.00	80.00
MMCA [41]	RN50+DETR / BERT-B	RGB	44.15	48.14	42.31	56.32	34.43	44.44	58.70	38.63	65.98	51.98	40.19	20.00	60.00
HiVG-B [35]	CLIP-B / CLIP-B	RGB	60.91	66.28	63.46	68.69	62.30	50.00	80.43	56.23	74.23	65.84	58.57	66.67	83.33
HiVG-L [35]	CLIP-L / CLIP-L	RGB	61.70	64.42	65.38	68.18	56.56	55.56	81.52	57.12	73.71	64.36	59.05	66.67	83.33
OneRef-B [36]	BEIT3-B / BEIT3-B	RGB	59.33	62.56	61.54	65.82	57.38	55.56	79.35	53.71	72.68	63.86	55.24	50.00	83.33
OneRef-L [36]	BEIT3-L / BEIT3-L	RGB	61.76	66.98	65.38	67.85	54.10	44.44	78.26	56.97	76.29	64.85	61.43	33.33	83.33
TransVG [6]	RN50+DETR / BERT-B	TIR	50.42	53.95	51.92	60.94	43.44	38.89	56.52	45.40	69.59	56.44	47.62	50.00	83.33
CLIP-VG [33]	CLIP-B / CLIP-B	TIR	32.55	26.28	19.23	36.87	23.77	22.22	42.39	24.18	40.72	35.64	20.95	0.00	16.67
D-MDETR [29]	CLIP-B / CLIP-B	TIR	52.88	59.77	67.31	61.05	39.34	50.00	60.87	47.99	75.26	55.45	43.06	80.00	60.00
D-MDETR [29]	RN50+DETR / BERT-B	TIR	47.91	51.16	57.69	60.54	40.16	38.89	58.70	41.46	71.13	55.94	38.28	20.00	80.00
MMCA [41]	RN50+DETR / BERT-B	TIR	43.54	46.28	48.08	54.30	33.61	44.44	48.91	37.44	67.01	50.50	35.89	40.00	60.00
HiVG-B [35]	CLIP-B / CLIP-B	TIR	58.24	63.95	65.38	65.99	51.64	38.89	72.83	50.89	73.71	62.87	51.43	50.00	83.33
HiVG-L [35]	CLIP-L / CLIP-L	TIR	58.79	61.16	67.31	63.64	52.46	55.56	67.39	50.89	71.13	63.37	51.43	50.00	66.67
OneRef-B [36]	BEIT3-B / BEIT3-B	TIR	52.79	50.93	44.23	60.10	47.54	44.44	58.70	44.51	69.59	54.95	46.67	50.00	83.33
OneRef-L [36]	BEIT3-L / BEIT3-L	TIR	59.09	63.72	65.38	65.15	51.64	50.00	77.17	53.56	77.32	58.42	50.95	83.33	66.67
MV-TransVG	RN50+DETR / BERT-B	RGB+TIR	51.52	54.19	53.85	64.48	45.90	50.00	61.96	45.40	71.65	59.41	49.52	66.67	66.67
MV-CLIP-VG	CLIP-B / CLIP-B	RGB+TIR	48.24	47.67	40.38	52.69	36.07	22.22	56.52	42.88	59.79	50.99	35.24	33.33	66.67
MV-D-MDETR	CLIP-B / CLIP-B	RGB+TIR	55.55	62.09	69.23	63.74	43.44	50.00	64.13	50.67	75.77	57.92	50.72	40.00	80.00
MV-D-MDETR	RN50+DETR / BERT-B	RGB+TIR	51.79	55.58	59.62	63.41	41.80	50.00	59.78	48.44	73.71	60.40	42.58	40.00	60.00
MV-MMCA	RN50+DETR / BERT-B	RGB+TIR	53.12	56.51	55.77	63.07	45.08	50.00	58.70	46.36	70.10	59.41	44.98	60.00	80.00
MV-HiVG-B	CLIP-B / CLIP-B	RGB+TIR	64.42	71.40	75.00	70.20	63.11	50.00	85.87	58.75	78.35	68.32	61.43	66.67	83.33
MV-HiVG-L	CLIP-L / CLIP-L	RGB+TIR	62.42	65.58	67.31	66.50	61.48	50.00	72.83	57.42	74.23	67.33	58.10	66.67	83.33
MV-OneRef-B	BEIT3-B / BEIT3-B	RGB+TIR	58.73	64.88	69.23	66.84	57.38	44.44	75.00	53.86	73.71	60.89	54.76	66.67	66.67
MV-OneRef-L	BEIT3-L / BEIT3-L	RGB+TIR	61.88	65.81	67.31	68.86	54.10	50.00	78.26	55.49	76.29	62.87	55.71	83.33	83.33
RGBT-VGNet (Ours)	CLIP-B / CLIP-B	RGB+TIR	64.97	68.37	73.08	70.37	63.11	44.44	78.26	62.31	79.38	69.80	62.38	66.67	83.33

Table 11. **Acc@0.5 across four weather conditions** (Cloudy, Foggy, Rainy, Sunny) for RefFLIR, RefM3FD, and RefMFAD. All methods, backbones, and modalities are included, following the style of Table 4 and Table 5 in the manuscript.

Method	Visual / Language Backbone	Modality	RefFLIR (Weather)				RefM3FD (Weather)				RefMFAD (Weather)			
			FY	RY	SY	CY	FY	RY	SY	CY	FY	RY	SY	CY
a. Pretrained model zero-shot transfer setting:														
CLIP-VG [33]	CLIP-B / CLIP-B	RGB	3.48	5.26	9.65	6.28	4.55	6.90	9.79	8.86	5.84	4.35	9.27	8.19
HiVG-B [35]	CLIP-B / CLIP-B	RGB	26.96	44.74	36.14	31.15	36.36	33.07	29.79	30.96	17.05	18.94	25.17	20.14
HiVG-L [35]	CLIP-L / CLIP-L	RGB	30.43	52.63	49.39	32.79	52.45	56.27	52.54	52.72	35.35	28.26	44.04	43.08
OneRef-B [36]	BEIT3-B / BEIT3-B	RGB	29.57	44.74	46.13	32.24	39.16	42.79	37.96	40.10	25.40	23.29	31.13	32.27
OneRef-L [36]	BEIT3-L / BEIT3-L	RGB	33.04	44.74	55.23	37.70	43.36	50.47	45.92	46.86	33.18	28.57	40.40	38.75
CLIP-VG [33]	CLIP-B / CLIP-B	TIR	4.35	13.16	8.83	7.10	8.39	7.99	3.31	8.93	3.09	2.80	7.62	4.48
HiVG-B [35]	CLIP-B / CLIP-B	TIR	13.91	36.84	11.75	13.93	18.53	16.93	10.21	9.14	5.95	4.04	11.92	8.01
HiVG-L [35]	CLIP-L / CLIP-L	TIR	20.43	44.74	24.86	24.59	30.77	41.07	27.75	25.73	20.48	16.77	33.11	23.53
OneRef-B [36]	BEIT3-B / BEIT3-B	TIR	20.87	42.11	27.92	24.04	20.63	27.59	21.20	22.80	12.13	10.25	23.18	16.53
OneRef-L [36]	BEIT3-L / BEIT3-L	TIR	25.65	57.89	27.31	24.32	30.77	29.47	20.28	23.08	16.93	15.22	21.19	18.06
b. Single source dataset training setting:														
TransVG [6]	RN50+DETR / BERT-B	RGB	34.35	47.37	45.45	34.70	52.10	44.51	36.27	39.54	47.03	44.41	63.58	48.25
CLIP-VG [33]	CLIP-B / CLIP-B	RGB	18.26	36.84	27.31	16.94	31.12	35.89	29.58	30.61	34.67	30.12	51.66	37.65
D-MDETR [29]	CLIP-B / CLIP-B	RGB	40.00	54.05	53.91	37.98	56.49	54.55	46.79	50.35	56.64	51.24	77.15	59.40
D-MDETR [29]	RN50+DETR / BERT-B	RGB	38.26	48.65	48.81	30.87	-	-	-	-	50.34	41.93	64.57	51.13
MMCA [41]	RN50+DETR / BERT-B	RGB	35.65	51.35	51.67	34.43	-	-	-	-	45.88	36.65	63.25	46.10
HiVG-B [35]	CLIP-B / CLIP-B	RGB	49.13	63.16	71.74	53.01	70.28	67.71	63.59	65.55	58.58	54.66	78.48	63.66
HiVG-L [35]	CLIP-L / CLIP-L	RGB	59.13	68.42	74.80	59.29	67.83	67.08	65.70	66.53	58.70	54.97	75.83	63.87
OneRef-B [36]	BEIT3-B / BEIT3-B	RGB	50.43	55.26	66.92	51.37	70.28	69.28	65.21	68.34	56.64	52.80	74.50	61.36
OneRef-L [36]	BEIT3-L / BEIT3-L	RGB	53.91	60.53	70.04	52.19	67.13	68.34	62.68	63.67	59.15	54.97	77.48	63.91
TransVG [6]	RN50+DETR / BERT-B	TIR	36.96	44.74	45.92	34.15	58.39	54.23	42.39	47.56	50.34	47.20	68.54	51.86
CLIP-VG [33]	CLIP-B / CLIP-B	TIR	35.22	47.37	38.72	32.79	33.92	34.64	23.31	26.22	29.75	24.53	40.07	30.84
D-MDETR [29]	CLIP-B / CLIP-B	TIR	41.74	54.05	48.40	40.44	64.56	53.29	45.45	51.05	54.69	45.65	69.87	53.93
D-MDETR [29]	RN50+DETR / BERT-B	TIR	47.83	51.35	43.44	39.07	-	-	-	-	50.00	42.55	66.23	49.16
MMCA [41]	RN50+DETR / BERT-B	TIR	46.52	45.95	42.28	35.79	-	-	-	-	45.42	38.82	60.93	44.28
HiVG-B [35]	CLIP-B / CLIP-B	TIR	63.04	73.68	56.79	59.29	77.97	69.28	57.82	62.90	58.70	49.07	73.84	59.32
HiVG-L [35]	CLIP-L / CLIP-L	TIR	66.09	76.32	64.67	69.13	81.12	72.88	56.97	63.74	58.58	53.11	72.52	58.23
OneRef-B [36]	BEIT3-B / BEIT3-B	TIR	58.26	68.42	60.46	60.93	77.62	71.94	59.65	64.99	51.49	47.20	67.22	52.15
OneRef-L [36]	BEIT3-L / BEIT3-L	TIR	60.43	65.79	61.96	60.93	81.12	73.20	61.97	69.87	59.15	53.73	71.19	60.01
MV-TransVG	RN50+DETR / BERT-B	RGB+TIR	40.87	55.26	48.98	38.80	59.44	53.92	43.59	47.63	52.17	45.96	71.85	53.42
MV-CLIP-VG	CLIP-B / CLIP-B	RGB+TIR	33.04	47.37	43.34	35.25	45.80	46.24	34.44	38.77	44.28	38.82	60.60	48.18
MV-D-MDETR	CLIP-B / CLIP-B	RGB+TIR	41.74	56.76	50.44	40.44	58.25	50.16	42.35	46.65	55.15	49.07	74.83	57.14
MV-D-MDETR	RN50+DETR / BERT-B	RGB+TIR	43.91	59.46	49.97	42.62	61.05	51.57	39.04	46.37	54.23	46.89	68.54	53.46
MV-MMCA	RN50+DETR / BERT-B	RGB+TIR	43.91	62.16	52.07	39.89	54.04	54.55	43.20	48.19	53.20	46.58	69.21	54.08
MV-HiVG-B	CLIP-B / CLIP-B	RGB+TIR	63.04	73.68	69.23	65.57	82.17	75.71	65.70	71.48	64.07	60.56	77.81	66.24
MV-HiVG-L	CLIP-L / CLIP-L	RGB+TIR	70.00	73.68	75.48	74.04	81.82	75.71	68.38	72.04	60.76	55.90	73.84	63.77
MV-OneRef-B	BEIT3-B / BEIT3-B	RGB+TIR	56.96	73.68	64.88	54.10	74.83	66.30	60.42	65.48	58.35	50.31	74.17	61.14
MV-OneRef-L	BEIT3-L / BEIT3-L	RGB+TIR	52.17	65.79	64.47	53.83	80.42	72.73	65.00	70.92	59.95	53.11	77.81	63.22
RGBT-VGNet (Ours)	CLIP-B / CLIP-B	RGB+TIR	65.65	78.95	75.61	67.49	84.97	79.47	68.87	75.59	65.22	62.11	77.81	66.53

Table 12. **Acc@0.5 across four illumination conditions** (Strong, Normal, Weak, Very Weak) on RefFLIR, RefM3FD, and RefMFAD for all methods, backbones, and modalities.

Method	Visual / Language Backbone	Modality	RefFLIR (Illumination)				RefM3FD (Illumination)				RefMFAD (Illumination)			
			VL	WL	NL	SL	VL	WL	NL	SL	VL	WL	NL	SL
a. Pretrained model zero-shot transfer setting:														
CLIP-VG [33]	CLIP-B / CLIP-B	RGB	12.50	5.13	0.00	9.69	12.86	8.77	8.48	6.70	8.33	6.92	8.20	16.67
HiVG-B [35]	CLIP-B / CLIP-B	RGB	37.50	30.29	50.00	36.15	48.57	34.02	30.31	22.68	22.22	19.90	19.59	0.00
HiVG-L [35]	CLIP-L / CLIP-L	RGB	50.00	32.85	50.00	49.45	65.71	56.73	51.65	50.00	27.78	38.02	43.97	16.67
OneRef-B [36]	BEIT3-B / BEIT3-B	RGB	37.50	31.89	66.67	46.04	54.29	48.25	36.37	30.93	25.00	28.28	32.76	0.00
OneRef-L [36]	BEIT3-L / BEIT3-L	RGB	50.00	36.22	66.67	55.25	52.86	52.92	44.90	37.63	36.11	35.20	39.40	0.00
CLIP-VG [33]	CLIP-B / CLIP-B	TIR	12.50	6.41	0.00	8.87	12.86	11.01	4.98	1.55	5.56	4.02	4.58	16.67
HiVG-B [35]	CLIP-B / CLIP-B	TIR	37.50	15.06	16.67	11.73	18.57	18.13	9.00	6.19	2.78	6.88	8.59	0.00
HiVG-L [35]	CLIP-L / CLIP-L	TIR	37.50	24.20	16.67	24.90	52.86	36.35	26.25	25.77	25.00	20.19	26.95	0.00
OneRef-B [36]	BEIT3-B / BEIT3-B	TIR	25.00	23.88	33.33	27.97	35.71	32.75	18.81	17.53	16.67	13.47	18.53	0.00
OneRef-L [36]	BEIT3-L / BEIT3-L	TIR	50.00	26.28	33.33	27.35	24.29	34.11	19.98	14.95	19.44	16.38	19.81	0.00
b. Single source dataset training setting:														
TransVG [6]	RN50+DETR / BERT-B	RGB	87.50	34.62	66.67	45.43	38.57	46.59	38.38	28.35	44.44	46.52	51.95	33.33
CLIP-VG [33]	CLIP-B / CLIP-B	RGB	25.00	18.59	33.33	27.22	31.43	40.25	27.89	25.26	33.33	34.41	41.69	16.67
D-MDETR [29]	CLIP-B / CLIP-B	RGB	62.50	39.26	66.67	53.89	50.72	57.46	47.91	40.72	60.00	55.87	64.17	100.00
D-MDETR [29]	RN50+DETR / BERT-B	RGB	87.50	33.81	66.67	48.77	-	-	-	-	51.43	48.73	54.58	50.00
MMCA [41]	RN50+DETR / BERT-B	RGB	75.00	35.26	66.67	51.64	-	-	-	-	45.71	43.92	50.11	50.00
HiVG-B [35]	CLIP-B / CLIP-B	RGB	87.50	51.76	66.67	71.76	71.43	69.40	64.23	59.79	55.56	59.83	67.24	83.33
HiVG-L [35]	CLIP-L / CLIP-L	RGB	87.50	59.46	66.67	74.83	77.14	69.20	65.55	58.76	66.67	60.28	66.46	83.33
OneRef-B [36]	BEIT3-B / BEIT3-B	RGB	87.50	50.80	66.67	66.92	84.29	71.44	66.08	58.25	66.67	57.55	64.73	50.00
OneRef-L [36]	BEIT3-L / BEIT3-L	RGB	87.50	52.88	66.67	70.05	78.57	69.49	62.42	56.70	61.11	59.49	68.14	83.33
TransVG [6]	RN50+DETR / BERT-B	TIR	75.00	35.26	66.67	45.91	54.29	55.75	45.14	32.99	52.78	49.83	55.64	83.33
CLIP-VG [33]	CLIP-B / CLIP-B	TIR	62.50	34.13	66.67	38.61	35.71	38.89	22.79	18.56	33.33	28.73	33.48	33.33
D-MDETR [29]	CLIP-B / CLIP-B	TIR	50.00	41.51	66.67	48.36	55.07	57.85	48.15	37.11	48.57	51.80	58.37	83.33
D-MDETR [29]	RN50+DETR / BERT-B	TIR	87.50	42.31	66.67	43.34	-	-	-	-	42.86	48.03	52.90	50.00
MMCA [41]	RN50+DETR / BERT-B	TIR	87.50	39.58	66.67	42.22	-	-	-	-	45.71	42.93	48.44	50.00
HiVG-B [35]	CLIP-B / CLIP-B	TIR	87.50	61.22	66.67	56.75	80.00	70.66	60.57	51.55	52.78	56.84	63.00	83.33
HiVG-L [35]	CLIP-L / CLIP-L	TIR	100.00	<u>67.95</u>	83.33	64.60	68.57	73.29	61.17	50.52	52.78	57.09	61.55	50.00
OneRef-B [36]	BEIT3-B / BEIT3-B	TIR	87.50	60.10	83.33	60.37	88.57	72.03	62.50	53.61	47.22	50.83	55.25	66.67
OneRef-L [36]	BEIT3-L / BEIT3-L	TIR	87.50	60.74	66.67	61.94	80.00	75.05	66.32	54.12	55.56	57.63	63.50	83.33
MV-TransVG	RN50+DETR / BERT-B	RGB+TIR	87.50	39.90	66.67	48.91	54.29	55.46	45.66	37.63	44.44	51.37	57.42	83.33
MV-CLIP-VG	CLIP-B / CLIP-B	RGB+TIR	50.00	34.94	66.67	43.25	42.86	50.58	34.61	30.93	50.00	45.02	50.84	50.00
MV-D-MDETR	CLIP-B / CLIP-B	RGB+TIR	62.50	41.51	66.67	50.41	50.72	54.05	44.17	35.05	60.00	53.84	61.94	100.00
MV-D-MDETR	RN50+DETR / BERT-B	RGB+TIR	75.00	43.59	66.67	49.93	46.38	54.34	43.01	32.47	60.00	52.01	57.03	50.00
MV-MMCA	RN50+DETR / BERT-B	RGB+TIR	87.50	41.99	66.67	52.05	49.28	57.27	44.94	34.54	54.29	51.51	58.31	50.00
MV-HiVG-B	CLIP-B / CLIP-B	RGB+TIR	87.50	64.74	66.67	69.24	92.86	77.19	68.45	59.79	63.89	<u>63.10</u>	70.37	66.67
MV-HiVG-L	CLIP-L / CLIP-L	RGB+TIR	87.50	72.28	83.33	<u>75.44</u>	87.14	<u>77.68</u>	<u>69.98</u>	<u>62.89</u>	<u>63.89</u>	60.78	66.52	83.33
MV-OneRef-B	BEIT3-B / BEIT3-B	RGB+TIR	87.50	55.77	66.67	64.87	78.57	68.91	63.06	53.09	58.33	57.71	64.62	66.67
MV-OneRef-L	BEIT3-L / BEIT3-L	RGB+TIR	75.00	53.69	66.67	64.46	81.43	74.76	68.17	58.76	61.11	59.49	67.19	83.33
RGBT-VGNet (Ours)	CLIP-B / CLIP-B	RGB+TIR	87.50	67.31	<u>66.67</u>	75.65	90.00	81.48	71.74	64.95	66.67	64.22	<u>70.03</u>	<u>83.33</u>

Table 13. **Acc@0.5 across object sizes** (Normal Size vs Small Size) and **different occlusion levels** (No-or-Partial vs Heavy) for RefFLIR, RefM3FD, and RefMFAD.

Method	Visual / Language Backbone	Modality	RefFLIR (Size and Occ)				RefM3FD (Size and Occ)				RefMFAD (Size and Occ)			
			NS	SS	PO	HO	NS	SS	PO	HO	NS	SS	PO	HO
a. Pretrained model zero-shot transfer setting:														
CLIP-VG [33]	CLIP-B / CLIP-B	RGB	14.44	1.11	11.36	4.12	15.46	1.35	12.09	4.03	16.88	1.22	12.41	4.52
HiVG-B [35]	CLIP-B / CLIP-B	RGB	62.06	2.23	48.48	25.66	56.12	5.30	42.01	23.08	46.53	1.92	42.20	17.87
HiVG-L [35]	CLIP-L / CLIP-L	RGB	75.97	7.81	60.61	29.92	85.53	19.59	76.43	40.35	81.76	12.86	69.86	32.20
OneRef-B [36]	BEIT3-B / BEIT3-B	RGB	74.47	3.55	55.30	28.86	74.59	3.19	59.63	29.22	70.82	2.86	60.28	25.66
OneRef-L [36]	BEIT3-L / BEIT3-L	RGB	77.20	17.04	59.85	38.70	77.59	14.72	69.26	34.53	73.71	12.35	67.73	28.09
CLIP-VG [33]	CLIP-B / CLIP-B	TIR	14.52	0.61	13.64	4.79	12.19	0.76	10.45	4.60	9.88	5.49	8.51	2.71
HiVG-B [35]	CLIP-B / CLIP-B	TIR	23.15	0.81	18.94	10.51	21.68	0.97	15.57	10.81	18.12	0.51	21.99	7.02
HiVG-L [35]	CLIP-L / CLIP-L	TIR	45.77	0.00	37.88	19.68	54.77	2.92	43.85	24.36	53.18	2.82	45.74	18.22
OneRef-B [36]	BEIT3-B / BEIT3-B	TIR	49.38	0.20	37.88	20.74	44.61	0.11	33.20	19.69	38.82	0.12	35.46	13.91
OneRef-L [36]	BEIT3-L / BEIT3-L	TIR	47.10	3.65	36.36	22.87	42.32	4.17	35.04	19.12	40.88	2.43	37.23	15.09
b. Single source dataset training setting:														
TransVG [6]	RN50+DETR / BERT-B	RGB	61.53	19.76	49.24	31.12	64.00	15.10	51.02	31.91	82.47	31.06	74.82	36.65
CLIP-VG [33]	CLIP-B / CLIP-B	RGB	40.85	15.81	27.27	16.22	55.86	5.39	42.42	22.51	72.71	13.16	63.48	27.89
D-MDETR [29]	CLIP-B / CLIP-B	RGB	68.75	26.77	54.55	37.10	73.29	26.08	65.78	38.87	87.00	40.98	78.72	45.97
D-MDETR [29]	RN50+DETR / BERT-B	RGB	64.52	20.95	50.00	34.04	-	-	-	-	82.24	30.41	74.47	37.20
MMCA [41]	RN50+DETR / BERT-B	RGB	68.49	21.50	54.55	33.64	-	-	-	-	76.94	26.24	71.28	33.31
HiVG-B [35]	CLIP-B / CLIP-B	RGB	85.39	43.52	75.76	52.66	90.51	45.04	84.84	54.41	90.41	45.57	86.17	50.14
HiVG-L [35]	CLIP-L / CLIP-L	RGB	89.08	50.00	81.06	59.31	92.84	41.29	87.70	56.65	91.82	44.98	87.94	51.60
OneRef-B [36]	BEIT3-B / BEIT3-B	RGB	85.21	35.90	75.76	49.07	92.79	39.07	87.30	58.44	90.24	40.86	86.17	48.47
OneRef-L [36]	BEIT3-L / BEIT3-L	RGB	86.27	39.76	72.73	52.26	92.89	34.52	84.63	54.92	90.12	45.18	85.46	49.72
TransVG [6]	RN50+DETR / BERT-B	TIR	61.27	21.18	50.76	32.98	71.52	22.51	64.14	37.98	83.76	31.37	78.72	38.46
CLIP-VG [33]	CLIP-B / CLIP-B	TIR	58.80	12.26	49.24	26.99	48.44	4.92	37.70	22.83	61.47	10.31	54.96	23.23
D-MDETR [29]	CLIP-B / CLIP-B	TIR	65.23	18.38	56.82	35.24	71.27	28.52	64.55	41.11	79.71	37.73	74.11	40.26
D-MDETR [29]	RN50+DETR / BERT-B	TIR	62.59	20.36	56.06	37.10	-	-	-	-	80.71	29.53	73.76	37.27
MMCA [41]	RN50+DETR / BERT-B	TIR	61.44	18.46	52.27	31.78	-	-	-	-	76.41	24.43	70.57	32.55
HiVG-B [35]	CLIP-B / CLIP-B	TIR	77.11	42.41	68.94	51.99	87.50	40.59	80.53	55.18	86.59	45.69	79.08	46.80
HiVG-L [35]	CLIP-L / CLIP-L	TIR	84.95	43.91	84.85	57.31	87.60	40.69	82.79	56.14	87.41	39.33	80.85	46.45
OneRef-B [36]	BEIT3-B / BEIT3-B	TIR	80.99	35.80	70.45	52.39	88.17	41.02	85.66	58.76	85.47	38.67	80.50	40.47
OneRef-L [36]	BEIT3-L / BEIT3-L	TIR	81.78	37.53	75.00	53.99	90.35	45.29	85.45	62.02	86.24	42.67	80.14	47.36
MV-TransVG	RN50+DETR / BERT-B	RGB+TIR	67.78	21.10	53.79	35.51	72.15	22.89	62.91	38.87	83.82	33.84	76.60	40.40
MV-CLIP-VG	CLIP-B / CLIP-B	RGB+TIR	64.44	16.06	50.00	29.79	66.60	10.01	54.71	30.43	82.82	23.96	74.82	36.93
MV-D-MDETR	CLIP-B / CLIP-B	RGB+TIR	68.40	23.38	56.06	36.70	67.89	24.19	60.66	38.04	84.24	39.30	75.89	43.32
MV-D-MDETR	RN50+DETR / BERT-B	RGB+TIR	68.22	24.52	62.88	37.90	68.41	21.81	60.25	35.49	83.94	34.24	75.18	40.75
MV-MMCA	RN50+DETR / BERT-B	RGB+TIR	71.92	22.62	59.85	37.10	74.07	20.45	64.14	37.72	84.76	34.16	77.66	41.31
MV-HiVG-B	CLIP-B / CLIP-B	RGB+TIR	86.36	50.20	78.03	56.91	92.74	49.40	89.55	63.55	91.24	51.53	89.72	54.03
MV-HiVG-L	CLIP-L / CLIP-L	RGB+TIR	90.23	51.16	83.33	66.22	94.09	44.74	90.37	65.03	90.71	42.36	86.88	51.32
MV-OneRef-B	BEIT3-B / BEIT3-B	RGB+TIR	80.99	35.43	70.45	52.39	88.17	37.93	85.66	58.76	85.47	41.58	80.50	40.47
MV-OneRef-L	BEIT3-L / BEIT3-L	RGB+TIR	83.19	35.09	71.97	51.20	92.17	46.27	87.50	62.34	88.94	45.25	81.21	49.72
RGBT-VGNet (Ours)	CLIP-B / CLIP-B	RGB+TIR	90.49	52.22	80.30	65.16	94.29	53.63	90.16	69.25	91.82	49.76	89.36	55.01